NJC

ROYAL SOCIETY OF CHEMISTRY

PAPER

View Article Online
View Journal | View Issue

Cite this: *New J. Chem.*, 2021, **45**, 13475

D–A dyads and A–D–A triads based on ferrocene: push–pull dyes with unusual behaviours in solution†

Guillaume Noirbent, *[a] Damien Brunel, *[a] Thanh-Tuân Bui, [b] Sébastien Péralta, [b] Pierre-Henri Aubert, [b] Didier Gigmes [a] and Frédéric Dumur *[a]

Received 6th April 2021,
Accepted 17th June 2021

DOI: 10.1039/d1nj01680f

rsc.li/njc

Ferrocene has been extensively used for the design of chromophores with reversible electrochemical properties. In this work, a series of twelve D–A dyads and twelve symmetrically substituted A–D–A triads have been developed based on twelve different electron acceptors. The photophysical characteristics of the different dyes have been studied using various techniques including UV-visible absorption and photoluminescence spectroscopy. Their electrochemical behaviours have also been determined. To evidence the specificities of the triads relative to those of their donor–acceptor (D–A) dyad analogues, comparison between these two families of dyes (D–A and A–D–A) has been made. The solvatochromic behaviour of the twenty-four dyes has been examined in 22 solvents of different polarities. Parallel to solvatochromism, suppression of the push–pull effect by oxidation of the ferrocene unit using a strong oxidizing agent, *i.e.* nitrosonium tetrafluoroborate, drastically modified the optical properties of the different dyes. To support the experimental results, theoretical calculations were carried out. Interestingly, in this work, an unprecedented modification of the UV-visible absorption spectra in solution was observed over time for all ferrocene-based push–pull dyes in various solvents. Evidence of this behaviour for ferrocene-based push–pull dyes is unprecedented in the literature.

1. Introduction

During the past few decades, push–pull dyes comprising an electron donor connected to an electron acceptor by means of a conjugated or a non-conjugated spacer have been extensively studied, due to the wide range of applications in which these different chromophores are involved.[1] Among the most popular applications, organic photovoltaics (OPVs),[2–7] organic field effect transistors (OFETs)[8] and non-linear optics (NLO)[9–13] can be cited as the most representative ones. However, emerging research fields such as visible light photopolymerization under low light intensity[14–23] and the blooming field of 3D-printing requiring dyes absorbing at 405 nm are also worth mentioning.[24,25] Compared to their inorganic counterparts, *i.e.*, the pigments that suffer from an incredible insolubility in common organic solvents, organic dyes offer several advantages such as easy tunability of their absorption maxima,[26–28] a facile processability due to their remarkable solubility in most of the common organic solvents, and an easy synthetic process, especially, if the Knoevenagel reaction is selected as the reaction used to form the conjugated spacer between the donor and the acceptor. For sub-disciplines[29,30] derived from NLO, such as bioimaging, non-linear frequency conversion of laser sources or electro-optic modulators, a fast response time is also required, which can be obtained with organic dyes and metal complexes such as ferrocene.[31–35] In numerous applications, organic dyes are often preferred over metal complexes due to the toxicity concerns raised by the use of metal-based dyes. However, non-toxic metals such as iron can be used to create push–pull dyes and one of the most representative complexes in this field is ferrocene.[36] This metallocene comprising an iron(II) cation sandwiched between two coplanar cyclopentadienyl cycles can be reversibly oxidized at a moderate potential so that this metallocene is internationally used as a reference for electrochemistry.[37] However, its scope of application is not limited to electrochemistry and ferrocene is now extensively used in medicine,[38] (photo)polymerization,[39,40] enantioselective catalysis,[41] for the design of molecular machines,[42] metal organic frameworks[43] and molecular rectifiers.[44] Due to its facile

[a] *Aix Marseille Univ, CNRS, ICR UMR 7273, F-13397 Marseille, France. E-mail: guillaume.noirbent@outlook.fr, damienbru@laposte.net, frederic.dumur@univ-amu.fr*
[b] *CY Cergy Paris Université, LPPI, F-95000 Cergy, France*

† Electronic supplementary information (ESI) available. See DOI: 10.1039/d1nj01680f

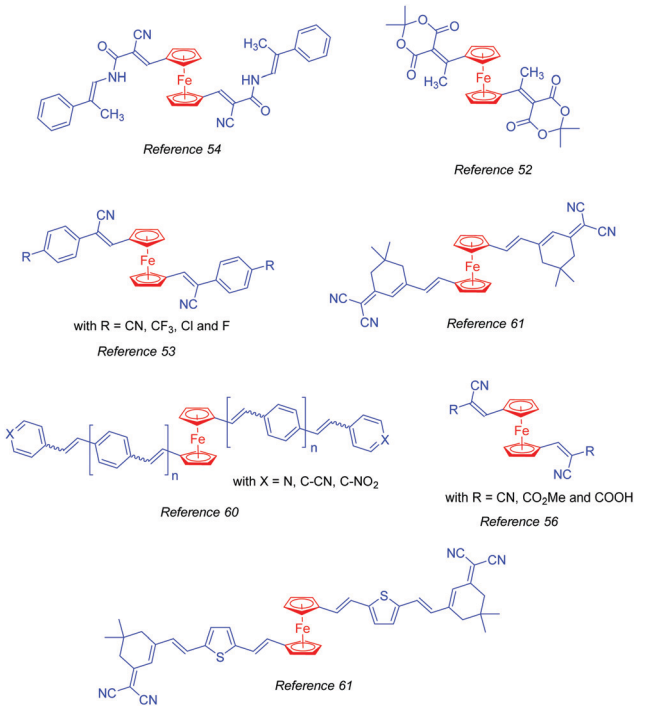

Fig. 1 Chemical structures of A–D–A ferrocene triads reported in the literature.

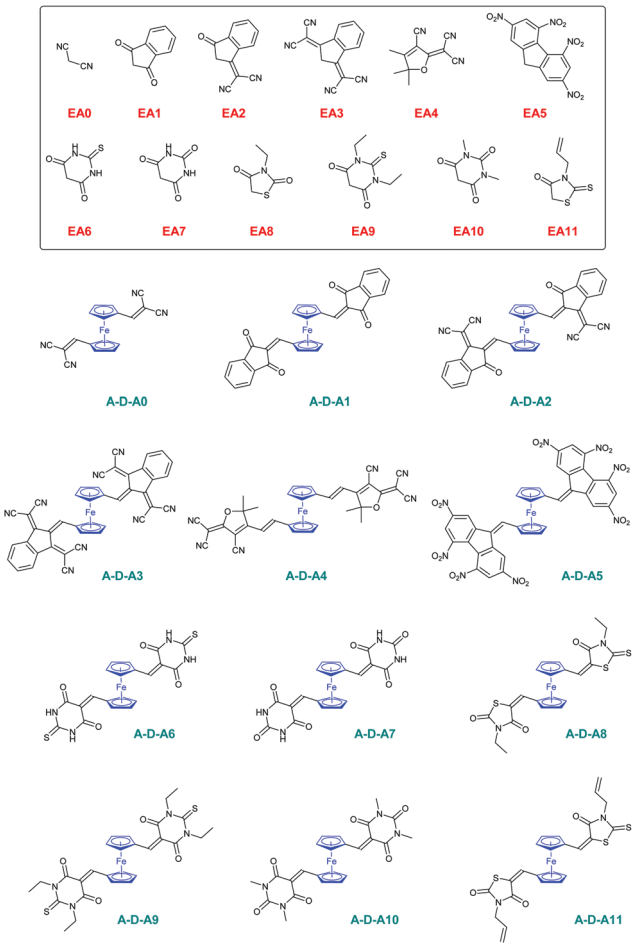

Fig. 2 Chemical structures of electron acceptors **EA*x***, x = 0–11 and A–D–A triads **A–D–A*x***, x = 0–11.

oxidation, ferrocene is also a good candidate for the design of donor–acceptor (D–A) conjugates and numerous dyads have been reported over the years.[45–55] Conversely, acceptor–donor–acceptor (A–D–A) triads based on ferrocene have only scarcely been examined in the literature (see Fig. 1).[56–61] In particular, the photophysical properties of A–D–A triads based on ferrocene have only been examined in detail in the case of Meldrum's derivatives (UV-visible absorption, fluorescence spectroscopy and spectroelectrochemistry).

Ferrocene possesses a low oxidation potential (0.52, 0.44 and 0.43 V *vs.* SCE in dichloromethane, acetonitrile, or DMF)[62] and can be thus oxidized to ferrocenium *via* a one-electron oxidation process.[63] This oxidation can not only be done electrochemically[64,65] but also chemically by using oxidizing agents such as nitrosonium tetrafluoroborate[66] or iron(III) sulfate.[67] One of the main advantages of nitrosonium tetrafluoroborate arises from its excellent solubility in common organic solvents, enabling to carry out the discoloration experiments in dichloromethane. Indeed, when ferrocene is used as an electron donor in push–pull structures, conversion of the electron-donating ferrocene to the electron-deficient ferrocenium can drastically affect the optical properties, as exemplified by A–D–A triads previously reported in the literature and comprising BODIPY and ferrocenes.[68] More generally, colour change is observed for all electrochromic devices comprising ferrocene as the electron-donating moiety.[69,70]

In this work, a series of twelve A–D–A triads comprising ferrocene-1,1′-dicarbaldehyde **ED2** as the electron donor have been synthesized and their photophysical properties have been determined (see Fig. 2). To evidence the main differences that exist between the twelve A–D–A triads (**A–D–A*x***, x = 0–11) and their twelve corresponding D–A dyads (**D–A*x***, x = 0–11), the latter ones have been synthesized with **EA0–EA11** as the electron acceptors and ferrocenecarboxaldehyde **ED1** as the donor for comparison (see Fig. 2). Parallel to the different investigations concerning their optical properties and their solvatochromic behaviour in solution, electrochemical measurements were also carried out to characterize the dyads and triads. Finally, by chemical oxidation of ferrocene to ferrocenium, suppression of the electron-donating part in the dyads and triads, and conversion of the electron-donating ferrocene as an electron acceptor (ferrocenium), a dramatic modification of their absorption spectra and colour changes of the solutions were observed. Modulation of the spectra obtained on oxidation has notably been previously examined in the literature, especially to demonstrate "switchable" NLO properties of ferrocene-based push–pull dyes.[71] In this work, for several compounds, the use of an excess of chemical oxidant resulted in successive oxidation processes that will be presented in this work. Finally, as one of the most interesting findings of this work, a modification of the optical properties of the ferrocene-based push–pull dyes in solution was demonstrated upon standing for the 24 dyes. This usual behaviour has never

been reported in the literature for ferrocene-based dyes, even if numerous dyads and triads comprising ferrocene as the electron donor have been reported in the literature.[45–59] This unusual behaviour was investigated using theoretical calculations, UV-visible absorption spectroscopy and cyclic voltammetry.

2. Experimental details

2.1. Materials and instrumentation methods

All reagents and solvents were purchased from Aldrich, Alfa Aesar or TCI Europe and used as received without further purification. Mass spectroscopy was performed at the Spectropole of Aix-Marseille University. ESI mass spectral analysis was recorded using a 3200 QTRAP (Applied Biosystems SCIEX) mass spectrometer. The HRMS mass spectral analysis was performed using a QStar Elite (Applied Biosystems SCIEX) mass spectrometer. Elemental analysis was performed using a Thermo Finnigan EA 1112 elemental analysis apparatus driven by the Eager 300 software. ^{1}H and ^{13}C NMR spectra were determined at room temperature in 5 mm o.d. tubes using a Bruker Avance 400 spectrometer of the Spectropole: ^{1}H (400 MHz) and ^{13}C (100 MHz). The ^{1}H chemical shifts were referenced to the solvent peak $CDCl_3$ (7.26 ppm) and the ^{13}C chemical shifts were referenced to the solvent peak $CDCl_3$ (77 ppm). UV-visible absorption spectra were recorded using a Varian Cary 50 Scan UV visible spectrophotometer, at concentration of 8×10^{-5} M, corresponding to diluted solutions. Fluorescence spectra were recorded using a Jasco FP 6200 spectrometer. The electrochemical properties of the investigated compounds were measured in dichloromethane by cyclic voltammetry, at a scan rate of 100 mV s^{-1}, with tetrabutylammonium perchlorate (0.1 M) as the supporting electrolyte in a standard one-compartment, three-electrode electrochemical cell under an argon stream using a VSP BioLogic potentiostat. The working, pseudo-reference and counter electrodes were platinum disk (Ø = 1 mm), Ag wire, and Au wire gauze, respectively. Ferrocene was used as an internal standard, and the potentials are referred to the reversible formal potential of this compound. Ferrocenecarboxaldehyde[72] **ED1**, ferrocene-1,1′-dicarbaldehyde[73] **ED2**, **D–A5** and **A–D–A5**[48] were synthesized as previously reported in the literature, without modification and in similar yields. Computational details: All quantum mechanical calculations were computed using Gaussian Package.[74] All geometry optimizations were performed using density functional theory (DFT) with the global hybrid exchange–correlation functional B3LYP[75] and all minima on the potential energy surface were verified *via* a calculation of vibrational frequencies, ensuring no imaginary frequencies were present. The Pople double-zeta basis set with a double set of polarization functions on non-hydrogen atoms (6-3111G(d,p))[76] was used throughout. This computational approach was chosen in consistency with previous works, as it provides good agreement with the experimental data. Excited states were probed using time dependent density functional theory (TD-DFT) using the same functional. All transitions (singlet–singlet) were calculated vertically with respect to the singlet ground state geometry. Solvent effects were taken into account by using the implicit polarizable continuum model (PCM).[77,78] DCM was chosen in analogy with the experiments. Computed spectra were simulated by convoluting each transition with Gaussian functions – centered on each absorption maximum – using a constant full width at half maximum (FWHM) value of 0.2 eV. The assignment of electronic transitions for λ_{max} has been determined using GaussSum 3.0 software.[79]

2.2. Synthesis of the dyes

2.2.1. General procedure used for the synthesis of D–A0–D–A11, except for D–A3 and D–A5. Electron acceptors **EA0–EA3** and **EA4–EA11** (5.79 mmol) and ferrocenecarboxaldehyde (1.24 g, 5.79 mmol, 1. eq.) were dissolved in absolute ethanol (50 mL) and a few drops of piperidine were added. Immediately, the solution colour changed. The solution was introduced in a preheated bath at 100 °C and the progress of the reaction was monitored by TLC. Typically, the reaction was stopped after 10 minutes. After cooling, a precipitate formed. It was filtered off, washed several times with ethanol and dried under vacuum.

2.2.2. General procedure used for the synthesis of D–A3. EA3 (5.79 mmol) and ferrocenecarboxaldehyde (1.24 g, 5.79 mmol, 1. eq.) were dissolved in acetic anhydride (50 mL) and the solution was refluxed overnight. After cooling, a precipitate formed. It was filtered off, washed several times with ethanol and dried under vacuum.

2.2.3. General procedure used for the synthesis of D–A5. EA5 (5.79 mmol) and ferrocenecarboxaldehyde (1.24 g, 5.79 mmol, 1. eq.) were dissolved in DMF (50 mL) and the solution was stirred at room temperature overnight. During this time, a precipitate formed. It was filtered off, washed several times with ethanol and dried under vacuum.

D–A0: EA0 (0.38 g, 5.79 mmol), m_{exp} = 1.49 g, 98% yield. ^{1}H NMR ($CDCl_3$) δ: 4.33 (s, 5H), 4.85 (s, 2H), 4.98 (s, 2H), 7.72 (s, 1H); ^{13}C NMR ($CDCl_3$) δ: 71.3, 71.9, 74.2, 75.4, 114.5, 115.3, 163.4; HRMS (ESI MS) *m*/*z*: theor: 262.0193 found: 262.0195 ($[M]^{+\bullet}$ detected).

D–A1: EA1 (0.85 g, 5.79 mmol), m_{exp} = 1.94 g, 98% yield. ^{1}H NMR ($CDCl_3$) δ: 4.23 (s, 5H), 4.84–4.85 (m, 2H), 5.43–5.44 (m, 2H), 7.75–7.79 (m, 2H), 7.88 (s, 1H), 7.93–7.97 (m, 2H); ^{13}C NMR ($CDCl_3$) δ: 70.7, 75.2, 75.3, 76.2, 77.2, 122.6, 122.8, 124.2, 134.5, 134.6, 139.9, 142.3, 149.4, 189.5, 190.5; HRMS (ESI MS) *m*/*z*: theor: 342.0343 found: 342.0342 ($[M]^{+\bullet}$ detected).

D–A2: EA2 (1.12 g, 5.79 mmol), m_{exp} = 2.20 g, 97% yield. ^{1}H NMR ($CDCl_3$) δ: 4.35 (s, 5H), 5.04 (s, 2H), 5.34 (s, 2H), 7.9–7.78 (m, 2H), 7.86–7.88 (m, 1H), 8.46 (s, 1H), 8.66 (d, 1H, J = 7.0 Hz); ^{13}C NMR ($CDCl_3$) δ: 68.1, 72.0, 76.9, 77.2, 77.7, 115.1, 115.3, 123.3, 123.6, 125.1, 134.2, 134.8, 137.3, 139.4, 149.6, 161.7, 187.2; HRMS (ESI MS) *m*/*z*: theor: 390.0456 found: 390.0455 ($[M]^{+\bullet}$ detected).

D–A3: EA3 (1.40 g, 5.79 mmol), m_{exp} = 1.1 g, 54% yield. ^{1}H NMR ($CDCl_3$) δ: 8.69–8.63 (m, 1H), 8.45 (s, 1H), 7.86 (dd, J = 6.1, 2.2 Hz, 1H), 7.76–7.69 (m, 2H), 5.35–5.29 (m, 2H), 5.06–5.01 (m, 2H), 4.34 (s, 5H); Anal. calc. for $C_{26}H_{14}FeN_4$: C, 71.2; H, 3.2; N, 12.8; found: C, 71.3; H, 3.3; N, 12.7%; HRMS (ESI MS) *m*/*z*: theor: 461.0460 found: 461.0462 ($[M + Na]^{+}$ detected).

D–A4: **EA4** (1.15 g, 5.79 mmol), m_{exp} = 1.86 g, 81% yield. ^{1}H NMR ($CDCl_3$) δ: 7.71 (d, J = 15.9 Hz, 1H), 6.49 (d, J = 15.9 Hz, 1H), 4.83 (s, 2H), 4.71 (s, 2H), 4.24 (s, 5H), 1.74 (s, 6H); ^{13}C NMR ($CDCl_3$) δ: 176.26, 173.28, 151.88, 111.16, 97.16, 79.29, 74.85, 71.22, 70.18, 26.51; HRMS (ESI MS) m/z: theor: 418.0613 found: 418.0611 ($[M + Na]^+$ detected).

D–A5: **EA5** (1.42 g, 5.79 mmol), m_{exp} = 2.76 g, 88% yield. ^{1}H NMR (Acetone-d_6) δ: 4.45 (s, 5H), 5.08 (t, 2H, J = 1.7 Hz), 5.18 (t, 2H, J = 1.7 Hz), 8.83 (d, 2H, J = 1.9 Hz), 8.96 (s, 1H), 9.47 (d, 1H, J = 1.9 Hz), 9.73 (d, 1H, J = 1.9 Hz); Anal. calc. for $C_{24}H_{14}FeN_4O_8$: C, 53.2; H, 2.6; O, 23.6; found: C, 53.3; H, 2.3; O, 23.7%; HRMS (ESI MS) m/z: theor: 565.0053 found: 565.0056 ($[M + Na]^+$ detected).

D–A6: **EA6** (0.84 g, 5.79 mmol), m_{exp} = 1.89 g, 96% yield. ^{1}H NMR ($CDCl_3$) δ: 8.48 (s, 1H), 5.36 (s, 2H), 5.10–5.07 (m, 2H), 4.33 (s, 5H); Anal. calc. for $C_{15}H_{12}FeN_2O_2S$: C, 52.9; H, 3.6; O, 9.4; found: C, 52.1; H, 3.6; O, 9.5%; HRMS (ESI MS) m/z: theor: 339.9969 found: 340.0002 ($[M]^{+\bullet}$ detected).

D–A7: **EA7** (0.74 g, 5.79 mmol), m_{exp} = 1.78 g, 95% yield. ^{1}H NMR ($CDCl_3$) δ: 8.47 (s, 1H), 5.34 (s, 2H), 5.00 (s, 2H), 4.30 (s, 5H); Anal. calc. for $C_{15}H_{12}FeN_2O_3$: C, 55.6; H, 3.7; O, 14.8; found: C, 55.5; H, 3.6; O, 14.5%; HRMS (ESI MS) m/z: theor: 324.0197 found: 324.0194 ($[M]^{+\bullet}$ detected).

D–A8: **EA8** (0.84 g, 5.79 mmol), m_{exp} = 1.77 g, 95% yield. ^{1}H NMR ($CDCl_3$) δ: 1.30 (t, 3H, J = 7.1 Hz), 4.17 (q, 2H, J = 7.1 Hz), 4.23 (s, 5H), 4.60 (s, 2H), 4.62 (s, 2H), 7.63 (s, 1H); ^{13}C NMR ($CDCl_3$) δ: 12.3, 39.7, 70.2, 71.0, 72.7, 118.9, 136.1, 142.1, 166.8, 192.9; HRMS (ESI MS) m/z: theor: 324.0197 found: 324.0194 ($[M]^{+\bullet}$ detected).

D–A9: **EA9** (1.16 g, 5.79 mmol), m_{exp} = 1.12 g, 49% yield. ^{1}H NMR ($CDCl_3$) δ: 8.44 (s, 1H), 5.48–5.22 (m, 2H), 5.13–4.90 (m, 2H), 4.56 (qd, J = 6.9, 1.7 Hz, 4H), 4.29 (s, 5H), 1.31 (td, J = 7.0, 2.8 Hz, 6H). ^{13}C NMR (75 MHz, $CDCl_3$) δ: 179.02, 162.13, 161.43, 159.02, 111.51, 71.29, 44.01, 43.39, 12.58; HRMS (ESI MS) m/z: theor: 419.0487 found: 419.0484 ($[M + Na]^+$ detected).

D–A10: **EA10** (0.90 g, 5.79 mmol), m_{exp} = 1.87 g, 92% yield. ^{1}H NMR ($CDCl_3$) δ: 3.36 (s, 3H), 3.39 (s, 3H), 4.27 (s, 5H), 4.89 (t, 2H, J = 1.9 Hz), 5.31 (t, 2H, J = 1.9 Hz), 8.44 (s, 1H); ^{13}C NMR ($CDCl_3$) δ: 28.2, 28.9, 71.0, 76.0, 76.3, 76.8, 110.7, 151.8, 161.0, 161.2, 163.3; HRMS (ESI MS) m/z: theor: 352.0510 found: 352.0513 ($[M]^{+\bullet}$ detected).

D–A11: **EA11** (1.00 g, 5.79 mmol), m_{exp} = 1.46 g, 68% yield. ^{1}H NMR ($CDCl_3$) δ: 7.64 (s, 1H), 5.94–5.81 (m, 1H), 5.36–5.21 (m, 2H), 4.73 (dt, J = 5.8, 1.4 Hz, 2H), 4.66–4.62 (m, 2H), 4.62–4.57 (m, 2H), 4.30–4.19 (m, 5H); ^{13}C NMR ($CDCl_3$) δ: 192.70, 166.68, 136.51, 129.81, 119.20, 118.63, 77.33, 77.22, 77.01, 76.69, 76.64, 72.84, 71.03, 70.26, 46.39; HRMS (ESI MS) m/z: theor: 391.9837 found: 391.9836 ($[M + Na]^+$ detected).

2.2.4. General procedure for the synthesis of A–D–A0–A–D–A11, excepted for A–D–A3 and A–D–A5. Ferrocene-1,1′-dicarbaldehyde (2 g, 8.26 mmol) and the appropriate electron acceptor **EA0–EA11** (16.52 mmol, 2 eq.) were suspended in ethanol and a few drops of piperidine were added. Immediately, the solution colour changed. The reaction was refluxed overnight. The solvent was removed under reduced pressure. The residue was purified by column chromatography (SiO_2) using a gradient of eluents from pentane to DCM for elution.

2.2.5. General procedure used for the synthesis of A–D–A3. **EA3** (5.79 mmol) and ferrocene-1,1′-dicarbaldehyde (0.70 g, 2.89 mmol) were dissolved in acetic anhydride (50 mL) and the solution was refluxed overnight. After cooling, a precipitate was formed. It was filtered off, washed several times with ethanol and dried under vacuum.

2.2.6. General procedure used for the synthesis of A–D–A5. **EA5** (5.79 mmol) and ferrocene-1,1′-dicarbaldehyde (0.70 g, 2.89 mmol) were dissolved in DMF (50 mL) and the solution was stirred at room temperature overnight. During this time, a precipitate was formed. It was filtered off, washed several times with ethanol and dried under vacuum.

A–D–A0: EA0 (1.1 g, 16.52 mmol), m_{exp} = 2.1 g, 75% yield. ^{1}H NMR ($CDCl_3$) δ: 7.63 (s, 2H), 5.09 (s, 4H), 4.89 (s, 4H). ^{13}C NMR ($CDCl_3$) δ: 160.58, 113.74, 113.31, 80.13, 75.72, 73.45, 29.69. HRMS (ESI MS) m/z: theor: 356.0593 found: 356.0592 ($[M + NH_4]^+$ detected).

A–D–A1: **EA1** (2.41 g, 5.79 mmol), m_{exp} = 1.90 g, 66% yield. ^{1}H NMR ($CDCl_3$) δ: 4.77 (s, 4H), 5.45 (s, 4H), 7.36 (s, 2H), 7.57–7.65 (m, 8H); ^{13}C NMR ($CDCl_3$) δ: 76.0, 76.7, 78.4, 122.6, 122.7, 126.3, 134.3, 134.5, 139.5, 141.9, 144.8, 188.7, 189.6; HRMS (ESI MS) m/z: theor: 498.0555 found: 498.0558 ($[M]^{+\bullet}$ detected).

A–D–A2: EA2 (3.2 g, 16.52 mmol), m_{exp} = 2 g, 41% yield. Anal. calc. for $C_{36}H_{18}FeN_4O_2$: C, 72.7; H, 3.0; O, 5.4; found: C, 72.5; H, 3.3; O, 5.7%; HRMS (ESI MS) m/z: theor: 617.0672 found: 617.0671 ($[M + Na]^+$ detected).

A–D–A3: EA3 (4.0 g, 16.52 mmol), m_{exp} = 0.55 g, 39% yield. Anal. calc. for $C_{42}H_{18}FeN_8$: C, 73.1; H, 2.6; N, 16.2; found: C, 73.3; H, 2.3; O, 16.4%; HRMS (ESI MS) m/z: theor: 797.0052 found: 797.0041 ($[M + Ag]^+$ detected).

A–D–A4: EA4 (3.3 g, 16.52 mmol), m_{exp} = 3 g, 91% yield. Anal. calc. for $C_{34}H_{24}FeN_6O_2$: C, 67.6; H, 4.0; O, 5.3; found: C, 67.7; H, 4.3; O, 5.4%; HRMS (ESI MS) m/z: theor: 627.1203 found: 627.1204 ($[M + Na]^+$ detected).

A–D–A5: EA5 (5.72 g, 16.52 mmol), m_{exp} = 12.17 g, 82% yield. Anal. calc. for $C_{38}H_{18}FeN_8O_{16}$: C, 50.8; H, 2.0; O, 28.5; found: C, 50.9; H, 2.1; O, 28.4%; HRMS (ESI MS) m/z: theor: 921.0082 found: 921.0086 ($[M + Na]^+$ detected).

A–D–A6: EA6 (2.12 g, 16.52 mmol), m_{exp} = 3.8 g, 99% yield. Anal. calc. for $C_{20}H_{14}FeN_4O_4S_2$: C, 48.6; H, 2.8; O, 12.9; found: C, 48.9; H, 2.9; O, 12.8%; HRMS (ESI MS) m/z: theor: 485.0155 found: 485.0156 ($[M + Na]^+$ detected).

A–D–A7: EA7 (2.38 g, 16.52 mmol), m_{exp} = 3.8 g, 93% yield. Anal. calc. for $C_{20}H_{14}FeN_4O_6$: C, 52.0; H, 3.0; O, 20.8; found: C, 51.9; H, 3.1; O, 20.6%; HRMS (ESI MS) m/z: theor: 494.9879 found: 494.9877 ($[M + Na]^+$ detected).

A–D–A8: EA8 (2.66 g, 16.52 mmol), m_{exp} = 3.48 g, 80% yield. ^{1}H NMR ($CDCl_3$) δ: 7.38 (s, 2H), 4.62 (m, 8H), 4.12 (d, J = 7.2 Hz, 4H), 1.28 (d, J = 7.1 Hz, 6H); ^{13}C NMR ($CDCl_3$) δ: 192.12, 166.78, 132.95, 121.66, 78.79, 73.84, 72.50, 39.98, 12.37. HRMS (ESI MS) m/z: theor: 550.9650 found: 550.9651 ($[M + Na]^+$ detected).

A–D–A9: EA9 (3.3 g, 16.52 mmol), m_{exp} = 3.6 g, 72% yield. ^{1}H NMR ($CDCl_3$) δ: 8.15 (s, 2H), 5.47 (s, 4H), 4.90–4.79 (m, 4H), 4.48 (q, J = 6.7 Hz, 8H), 1.27 (t, J = 6.6 Hz, 12H); ^{13}C NMR

($CDCl_3$) δ: 178.80, 160.88, 159.71, 158.65, 114.43, 78.75, 77.99, 77.20, 77.16, 44.12, 43.52, 12.48. HRMS (ESI MS) m/z: theor: 629.0951 found: 629.0951 ($[M + Na]^+$ detected).

A–D–A10: EA10 (2.58 g, 16.52 mmol), m_{exp} = 3.86 g, 90% yield. ^{1}H NMR ($CDCl_3$) δ: 8.05 (s, 2H), 5.44 (s, 4H), 4.81 (s, 4H), 3.32 (s, 12H); ^{13}C NMR ($CDCl_3$) δ: 162.58, 160.54, 157.79, 113.03, 78.46, 77.20, 76.60, 28.81, 28.15. HRMS (ESI MS) m/z: theor: 541.0781 found: 541.0779 ($[M + Na]^+$ detected).

A–D–A11: EA11 (2.86 g, 16.52 mmol), m_{exp} = 3.26 g, 72% yield. ^{1}H NMR ($CDCl_3$) δ: 7.41 (s, 2H), 5.86 (ddd, J = 16.3, 11.2, 5.9 Hz, 2H), 5.27 (t, J = 14.8 Hz, 4H), 4.75–4.53 (m, 12H); ^{13}C NMR ($CDCl_3$) δ: 190.75, 165.54, 132.13, 128.78, 120.32, 118.28, 77.60, 72.79, 71.42, 66.90, 45.53; Anal. calc. for $C_{24}H_{20}FeN_2O_3S_3$: C, 53.7; H, 3.8; O, 8.9; found: C, 53.9; H, 4.1; O, 8.6%; HRMS (ESI MS) m/z: theor: 574.9650 found: 574.9649 ($[M + Na]^+$ detected).

3. Results and discussion

3.1. Synthesis of the different dyes

The twelve D–A dyads **D–A*x***, x = 0–11 and the twelve triads **A–D–A*x***, x = 0–11 have been synthesized using a Knoevenagel condensation between the twelve electron acceptors **EA*x***, x = 0–11 and the two ferrocene donors **ED1** and **ED2**. All reactions were carried out using ethanol as the solvent and a catalytic amount of piperidine, excepted for all dyes comprising **EA3** and **EA5** as the electron acceptors (see Scheme 1). In the case of **EA3**, as **EA3** anion is highly stable and unreactive under basic conditions, **D–A3** and **A–D–A3** were prepared by refluxing **ED1** or **ED2** and **EA3** in acetic anhydride. The two dyes were obtained in 54 and 39% yields, respectively. Conversely, the methylene group of 2,4,5,7-tetranitro-9*H*-fluorene (TNF) is highly acidic so that this electron acceptor spontaneously deprotonates in highly polar solvents such as DMF. Consequently, **D–A5** and **A–D–A5** could be prepared in DMF, at room temperature without using any base. **D–A5** and **A–D–A5** could be obtained in 88 and 82% yields, respectively. Overall, the different dyes were obtained with reaction yields ranging from 39% for **A–D–A3** to 99% for **A–D–A6** (see Table 1). Interestingly, for dyes prepared in ethanol, the dyes were obtained as precipitates upon cooling of the ethanolic solutions so that the workup could be reduced to a simple filtration to recover the targeted products in pure form. Similarly, **D–A5** and **A–D–A5** could be obtained by precipitation from DMF whereas **D–A3** and **A–D–A3** precipitated from the acetic anhydride solutions.

3.2. Optical properties

3.2.1. Optical properties in chloroform. Optical data of dyads **D–A*x***, x = 0–11 and triads **A–D–A*x***, x = 0–11 are summarized in Table 2 and the UV-visible absorption spectra of all dyes recorded in chloroform are presented in Fig. 3, except for **A–D–A6** and **A–D–A7** for which their low solubilities in chloroform did not allow to determine their molar extinction coefficients with accuracy. Absorption spectra of all dyes were quite similar.

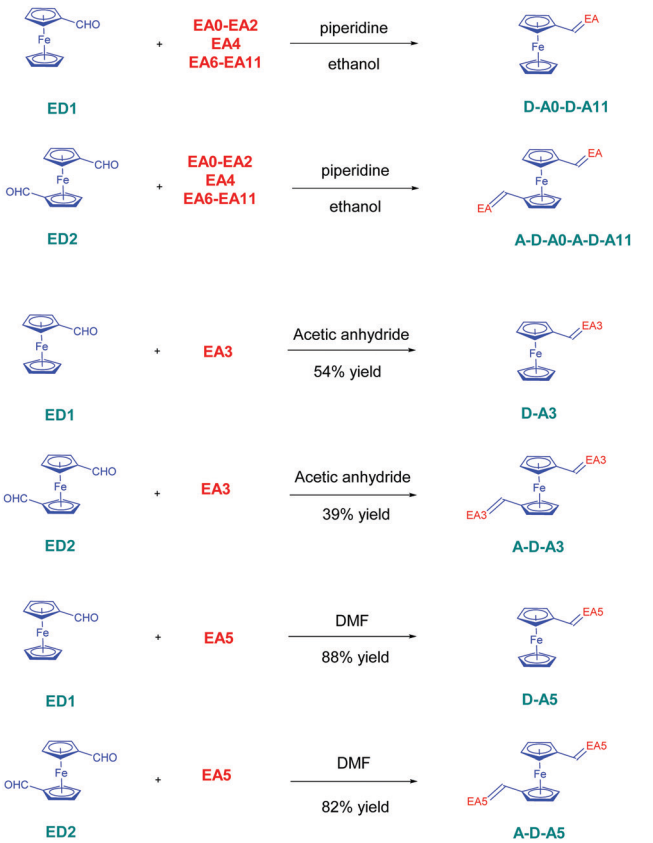

Scheme 1 Synthetic route to D–A dyads **D–A*x***, x = 0–11 and A–D–A triads **A–D–A*x***, x = 0–11.

As shown in Fig. 3, all dyes exhibited an intense absorption band centered in the visible range. This absorption band corresponds to the intramolecular charge transfer (ICT) band between the electron-donating ferrocene and the different electron-accepting groups.[80] However, recent works done on ferrocene-based push–pull dyes and especially theoretical calculations done on such structures by Barlow *et al.* have revealed this transition to be more

Table 1 Reaction yields obtained for the synthesis of dyads **D–A*x***, x = 0–11 and triads **A–D–A*x***, x = 0–11

Compounds	D–A0	D–A1	D–A2	D–A3	D–A4	D–A5
Reaction yields (%)	98	98	97	54[a]	81	88[b]
Compounds	D–A6	D–A7	D–A8	D–A9	D–A10	D–A11
Reaction yields (%)	96	95	95	49	92	68
Compounds	A–D–A0	A–D–A1	A–D–A2	A–D–A3	A–D–A4	A–D–A5
Reaction yields (%)	75	66	41	39[a]	91	82[b]
Compounds	A–D–A6	A–D–A7	A–D–A8	A–D–A9	A–D–A10	A–D–A11
Reaction yields (%)	99	93	80	72	90	72

[a] Reaction performed in acetic anhydride. [b] Reaction done in DMF.

Table 2 Summary of the UV-visible absorption characteristics of all dyads and triads in dilute chloroform

Compounds	λ_{max} (nm)	Epsilon (L mol^{-1} cm^{-1})	λ_{max} (ICT$_1$) (nm)	Epsilon (ICT) (L mol^{-1} cm^{-1})	ΔE (eV)
D–A0	326	13 980	531	2490	2.33
D–A1	361	25 070	571	6000	2.17
D–A2	319	24 180	629	6720	1.97
	413	12 200			
D–A3	318	14 000	623	3000	1.98
D–A4	424	24 890	630	9750	1.97
D–A5	366	43 700	607	7964	2.00
	427	20 300			
D–A6	377	24 900	583	5650	2.13
D–A7	356	20 300	565	4850	2.20
D–A8	382	26 920	542	6200	2.29
D–A9	377	31 900	583	7550	2.13
D–A10	353	21 700	558	5100	2.22
D–A11	382	26 150	542	6200	2.29
A–D–A0	341	17 700	445	2400	2.78
			533	2500	2.33
A–D–A1	375	18 500	572	6300	2.17
A–D–A2	314	30 200	580	4800	2.14
A–D–A3	—[a]	—[a]	632	6300	1.97
A–D–A4	311	12 300	603	1600	2.05
	412	4800			
A–D–A5	362	7500	616	1350	2.01
	429	3400			
A–D–A6	n.s.	n.s.	n.s.	n.s.	n.d.
A–D–A7	n.s.	n.s.	n.s.	n.s.	n.d.
A–D–A8	364	29 600	474	4750	2.62
	393	20 400	536	4300	2.31
A–D–A9	309	17 800	568	3100	2.18
	395	18 000			
A–D–A10	311	18 400	463	2900	2.67
	365	10 700	564	2450	2.20
A–D–A11	363	34 800	529	4843	2.34

n.s.: not soluble. [a] Peak detected below 300 nm.

complex than a simple HOMO → LUMO transition. Indeed, this optical transition detected at low energy corresponds to a transition originating between a set of degenerate HOMOs and the LUMO energy level.[81] The contributions of the different transitions in this absorption band is discussed later in this work.

A stronger absorption band can also be detected in the near-UV-visible range. By finely tuning the electron-accepting ability and by examining twelve electron acceptors (**EA0–EA11**), positions of the ICT bands could vary from 531 nm for **D–A0** exhibiting the weakest electron acceptor to 630 nm for **D–A3** comprising the strongest electron acceptor **EA3**. Interestingly, lower variations of the absorption maxima could be found for the absorption bands located in the near-UV-visible range than for the absorption band at low energy. Based on previous works reported in the literature, this transition was assigned to a transition between an occupied π-orbital consisting of a combination of highest occupied cyclopentadienyl orbital and highest occupied π bridge orbital and the LUMO energy level.[82] Considering the specificity of this transition detected at high energy, increase of the electron donating ability of the electron acceptor lowers both the energy levels of the LUMO and the energy level of the degenerated π-orbitals. Consequently, due to the similar variations of these two orbitals the position of this transition remained almost unchanged. Conversely, the HOMO level remains unaffected with increase in the acceptor strength so that a greater variation of the ICT band can be observed with increase in the electron-accepting ability of the acceptors.

Concerning the symmetrically substituted A–D–A triads, positions of the ICT bands varied from 533 nm for **A–D–A0** to 632 nm for **A–D–A3**. These results are consistent with the electron-withdrawing ability of the acceptors, malononitrile **EA0** being the weakest acceptor and 2,2′-(1*H*-indene-1,3(2*H*)-diylidene)dimalononitrile **EA3** being the strongest one. Interestingly, a decrease in the intensity of the charge transfer band was observed while going from D–A dyads to A–D–A triads.

Reduction of the molar extinction coefficients of the A–D–A triads relative to that of their dyad counterparts can be assigned to the fact that, in the case of A–D–A triads, the electron-donating ability of ferrocene is split between the two electron acceptors. On the contrary, the electronic delocalization is unidirectional in the D–A dyads, thus higher molar extinction coefficients can be measured due to the enhanced oscillating strength. However, geometry of D–A and A–D–A complexes have also to be considered to support these differences of molar extinction coefficients. Indeed, when only one cyclopentadienyl ring is functionalized in the case of D–A dyads, the free rotation existing between the two cyclopentadienyl rings of the A–D–A triads can position the two electron-accepting groups in parallel position, antiparallel position, or intermediate situation that can be hardly anticipated.[60] As a result of this, the conformational preferences in solution for the different dyes can also contribute to modify their molar extinction coefficients as well as the total dipole moment of the molecules. Noticeably, ICT band with the highest molar extinction coefficient for D–A dyads was determined for **D–A4** bearing 2-(3-cyano-4,5,5-trimethylfuran-2(5*H*)-ylidene)malononitrile (**EA4**, TCF) (ε = 9750 L mol^{-1} cm^{-1}) as the acceptor, whereas the highest molar extinction coefficient for the ICT band of the A–D–A triads was measured for **A–D–A3** (ε = 6300 L mol^{-1} cm^{-1}) possessing 2,2′-(1*H*-indene-1,3(2*H*)-diylidene)dimalononitrile **EA3** as the acceptor. Therefore, it can be concluded that the highest molar extinction coefficients were obtained with the strongest electron acceptors, inducing the highest electronic delocalization. Surprisingly, no clear trend could be established while comparing the maximum absorption of dyads and triads. Indeed, as observed for **D–A0**, **D–A1**, **D–A5**, **D–A8** and **D–A10**, almost no modification of the absorption maxima between dyads and triads was found. This result can be assigned to the weakness of the different electron acceptors used in these dyes so that the presence of one or two electron acceptors does not drastically affect the optical properties. Conversely, a hypsochromic shift was detected for the ICT bands of **A–D–A2**, **A–D–A4**, **A–D–A9** and **A–D–A11** compared to those of their diad analogues. Only **A–D–A3** (λ_{max} = 632 nm) showed a red-shifted absorption compared to **D–A3** (λ_{max} = 623 nm). These unexpected behaviors detected for **A–D–A*x***, x = 0–11 can be assigned to the presence of two broad absorption bands in the visible range with positions varying differently from one dye to another.

As shown in Fig. 4, three different situations could be found, affecting the determination of the absorption maxima for the

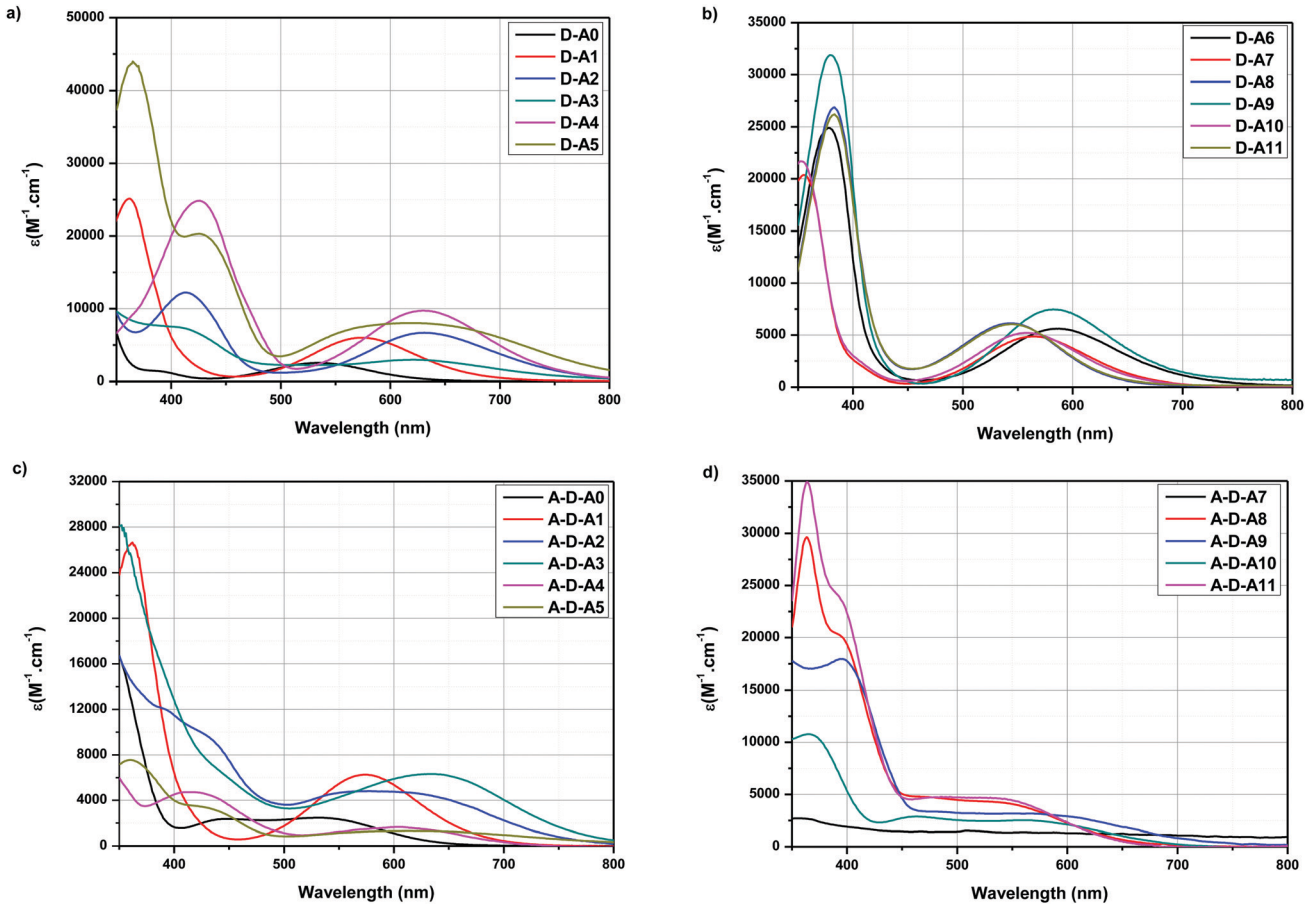

Fig. 3 UV-visible absorption spectra of D–A dyads **D–Ax**, *x* = 0–11 (a and b) and A–D–A triads **A–D–Ax**, *x* = 0–11 (c and d) in chloroform.

ICT band. Thus, to illustrate this, for **A–D–A0**, **A–D–A9** and **A–D–A10**, two distinct absorption bands could be detected in the visible range (400–600 nm) so that positions of the two bands could be easily determined. This situation was notably found for dyes prepared with malononitrile **EA0**, 1,3-diethyl-2-thioxodihydropyrimidine-4,6(1*H*,5*H*)-dione **EA9** and 1,3-dimethylpyrimidine-2,4,6(1*H*,3*H*,5*H*)-trione **EA10**. Conversely, for **A–D–A2**, a broad band extending from 500 to 700 nm could be evidenced, with no real presence of peaks so that the positions of the two bands could not be determined with accuracy. Such absorption

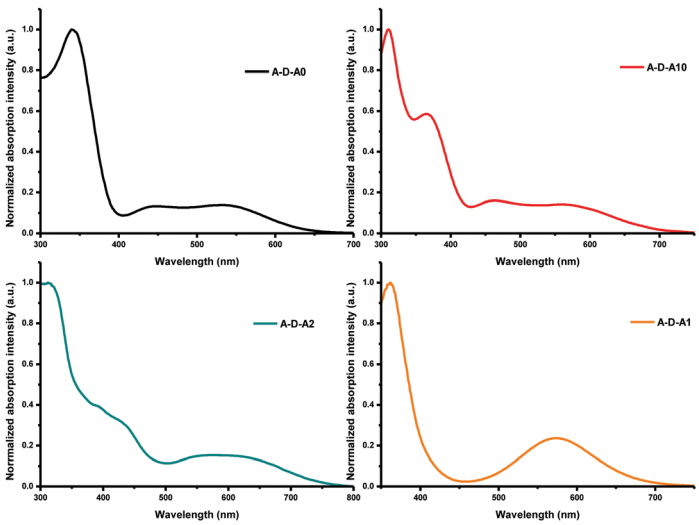

Fig. 4 Normalized UV-visible absorption spectra of A–D–A triads **A–D–A0**, **A–D–A1**, **A–D–A2** and **A–D–A10** in chloroform.

spectra were not only found for **A–D–A2** comprising 2-(3-oxo-2,3-dihydro-1*H*-inden-1-ylidene) malononitrile **EA2** but also for **A–D–A3**, **A–D–A4**, **A–D–A6**, **A–D–A8**, **A–D–A9** and **A–D–A11**. In terms of electron-accepting groups, 2,2′-(1*H*-indene-1,3(2*H*)-diylidene)dimalononitrile **EA3**, 2-(3-cyano-4,5,5-trimethylfuran-2(5*H*)-ylidene)malononitrile **EA4**, 2-thioxodihydropyrimidine-4,6(1*H*,5*H*)-dione **EA6**, 3-ethyl-thiazolidine-2,4-dione **EA8**, 1,3-diethyl-2-thioxo-dihydropyrimidine-4,6(1*H*,5*H*)-dione **EA9** and 3-allyl-2-thioxo-thiazolidin-4-one **EA11** drastically differ in their electron-withdrawing abilities. Except for **EA8** and **EA11**, **EA2** and **EA3**, and **EA6** and **EA9** that are of similar structures, **EA4** is the only representative of its category. In particular, if two ICT bands are found with indane-1,3-dione **EA2**, an overlap of the two bands can be found for **EA3** and **EA4**-based dyes (**A–D–A3** and **A–D–A4**), which can be related to the improvement of the electron-withdrawing ability in **EA3** and **EA4** compared to **EA2**. However, as counter-examples, **EA8** and **EA10** that are rhodanine-based acceptors are weaker acceptors than **EA2–EA4**. Therefore, no trend between electron-withdrawing ability and coalescence of the two ICT bands can be established. Finally, as observed for **A–D–A–1**, a coalescence of the bands within a unique absorption band was observed. This behaviour was also found for **A–D–A5** and **A–D–A7**. Here again, **A–D–A5** is the strongest electron-acceptor of the series whereas **EA7** is of comparable electron-withdrawing ability than **EA10**. Considering that **EA7** and **EA10** differ by the alkylation of the barbituric acceptor, once again, no trend between coalescence of the ICT bands or not and electron-withdrawing ability can be established. Considering the difficulty to determine with accuracy the positions of the ICT band of the lowest energy for A–D–A triads, the diversity of situations found for **A–D–A0–A–D–A11**, only the solvatochromism of the dyads **D–A*x***, x = 0–11 could be analyzed, due to the presence of a unique ICT band. Optical properties of the twenty-four dyes were also examined theoretically by performing density functional theory (DFT) calculations at the B3LYP/6-311G(d,p) level using the Gaussian09 program. For the different calculations, dichloromethane was selected as the solvent and a polarizable continuum model (PCM) was used to simulate the solvent. A summary of the optical properties is provided in the Table 3. As shown in Fig. 5, a redshift of the absorption spectra of all triads compared to that of dyads was predicted. A severe mismatch between the positions of the ICT bands determined experimentally and theoretically can also be evidenced. Thus, comparison of the absorption maxima for **D–A0** showed a difference as high as 100 nm between the experimental and theoretical values (λ_{exp} = 531 nm *vs.* λ_{th} = 632 nm). A higher disagreement between the theoretical and experimental values was found for the triads, resulting from the presence of two ICT bands. While examining the main contributions involved in the optical transitions detected at low energy for all dyes (see contributions in ESI†), these absorption bands clearly correspond to an admixture of numerous transitions and transitions occurring between HOMO−2 → LUMO, HOMO−2 → LUMO+1, HOMO−1 → LUMO+1, HOMO → LUMO, and HOMO → LUMO+1 can notably be cited. Additionally, contributions of each transition vary from one dye to another, it can thus support the mismatch existing between the theoretical and the experimental absorption spectra. Finally, examination of the photoluminescence properties of the different dyes revealed that these compounds are not emissive at all.

Table 3 Summary of the theoretical absorption characteristics of dyads and triads in dichloromethane

Compounds	λ_{max} (nm)	Epsilon (L mol^{-1} cm^{-1})	λ_{max} (ICT$_1$) (nm)	Epsilon (ICT) (L mol^{-1} cm^{-1})
D–A0	323	37 500	632	1350
D–A1	358	50 400	650	2400
D–A2	417	25 600	687	4000
D–A3	438	27 500	672	5000
D–A4	429	80 500	683	6200
D–A5	401	28 100	546	7700
			831	3300
D–A6	305 (sh)	4300	669	2500
	371	55 800		
D–A7	295 (sh)	6300	650	1800
	339	39 250		
D–A8	293	12 200	625	2400
	388	42 000		
D–A9	300	5450	659	2800
	374	56 700		
D–A10	250	7600	643	1900
	289	6400		
	338	42 800		
D–A11	294	10 900	623	2400
	388	41 900		
A–D–A0	351	59 000	712	1300
A–D–A1	394	43 500	745	2200
A–D–A2	450	52 000	520 (sh)	23 700
A–D–A3	492	16 200	751	3600
A–D–A4	477	96 300	765	5400
A–D–A5	458(sh)	8800	796	6600
	539	25 400		
A–D–A6	439	15 500	790	1700
A–D–A7	370	68 250	759	1150
A–D–A8	429	69 500	680	3200
A–D–A9	421	30 300	777	1700
A–D–A10	369	73 100	745	1300
A–D–A11	428	69 700	683	3100

This result is not surprising considering that ferrocene is commonly used to quench the photoluminescence of fluorescent dyes. In this field, a relevant example of this has recently been reported with a ferrocene–BODIPY dyad so that the photoluminescence of the highly emissive BODIPY could be efficiently quenched by ferrocene, due to photoinduced electron transfer.[83] In the present case, presumably, non-radiative pathways win out because (i) oscillator strengths are smaller than those in organic dyes, (ii) Fe leads to greater ISC rates than in typical organics, and perhaps (iii) because of the extra internal conversion pathways associated with rotation around the Cp–Fe–Cp bond.

3.2.2. Modification of the UV-visible absorption spectra of dyads and triads over time. The stability of dyes in solution is an important parameter that is required for numerous applications such as photopolymerization, non-linear optics and water waste treatment. In the literature, stability of dyes in solution under dark and light conditions has been extensively studied, especially for azo dyes,[84] polymethine dyes[85] and anthocyanins.[86,87] To date, this point has never been examined for ferrocene-based dyes, even when numerous reports can be found in the literature concerning dyes comprising ferrocene as the electron donor.[45–59] The stability

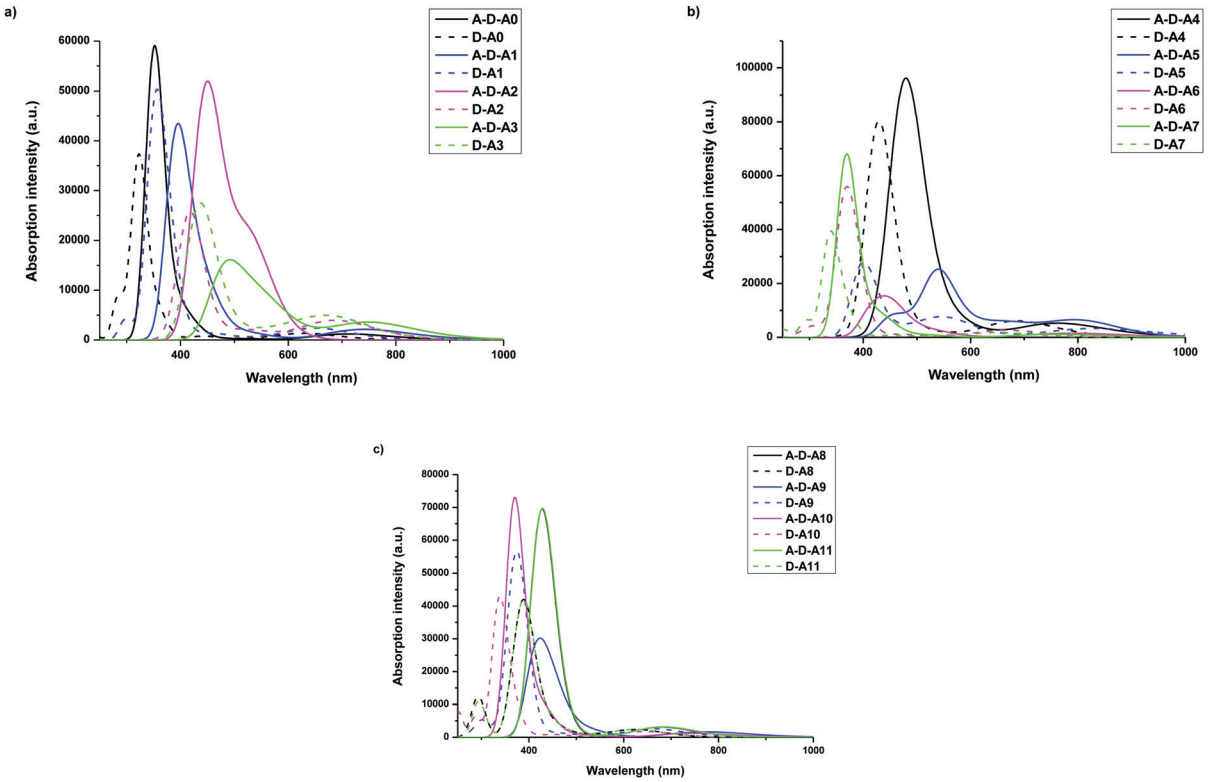

Fig. 5 Simulated absorption spectra of D–A dyads **D–Ax**, x = 0–11 and A–D–A triads **A–D–Ax**, x = 0–11 in dichloromethane.

of the twenty-four dyes in solution was thus examined by UV-visible absorption spectroscopy, first for **A–D–A0** to be used as a model compound. As shown in the Fig. 6, while no modification of the UV-visible absorption spectra of **A–D–A0** was found in anisole, 1,2-dichloroethane, dichloromethane, diglyme or toluene, a complete change of the UV-visible absorption spectra was found in solvents such as acetone, acetonitrile, ethyl acetate, chloroform, diethyl carbonate, dioxane, dimethylacetamide, DMF, DMSO, diethyl ether, THF or xylene. It is noteworthy that for this study, only solvents of HPLC grade were used and that no purification (distillation, dehydration, *etc.*) was carried out prior to analysis. All experiments were carried out at ambient temperature *i.e.* in the range of 18–20 °C. Face to these results, investigations were enlarged to all dyads **D–Ax**, x = 0–11 and triads **A–D–Ax**, x = 0–11 and DMSO was

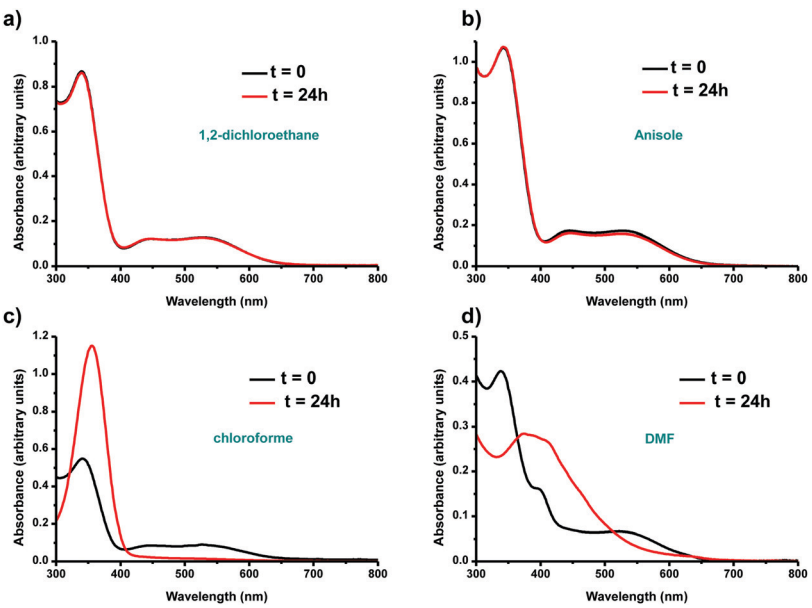

Fig. 6 Evolution of the UV-visible spectra of **A–D–A0** in different solvents over time.

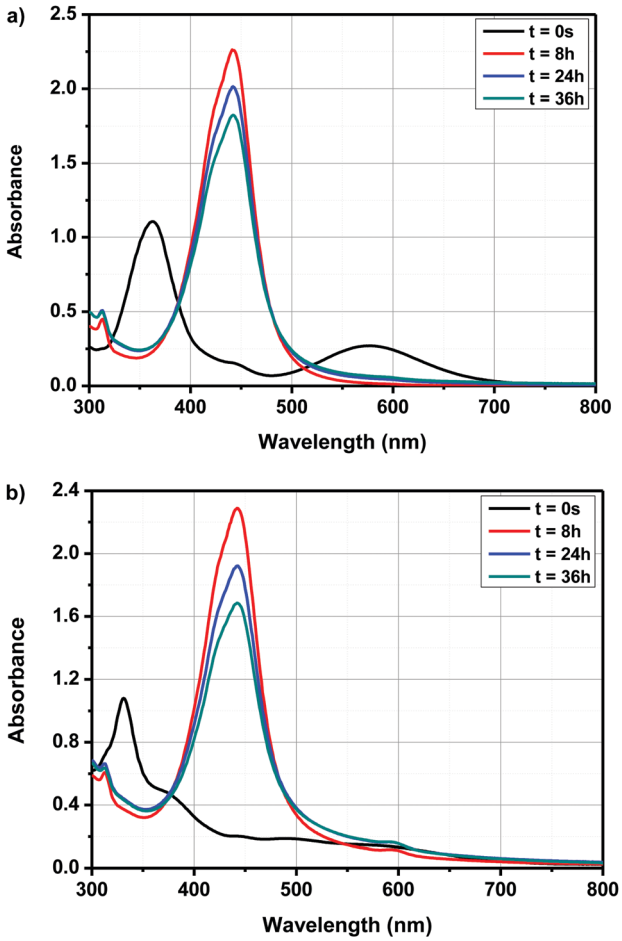

Fig. 7 Evolution of the UV-visible absorption spectra of **D–A1** and **A–D–A1** in DMSO over time.

considered as an appropriate solvent for this study, as all dyes were soluble in this solvent. Interestingly, a complete change of the UV-visible absorption spectra could be evidenced for the 24 dyes in DMSO (see Fig. 7). Conversely, control experiment done with ferrocene alone in DMSO revealed that its UV-visible absorption spectrum remains unchanged after 24 hours, not only in the dark, but also in ambient light. Therefore, the crucial role of the push–pull structure and the unavoidable role of the electron acceptors in these unexpected behaviors was clearly evidenced. Based on previous works reported in the literature, the ability of ferrocene to form a charge-transfer-to-solvent (CTTS) interaction with electron accepting solvents has been notably reported for solvents such as carbon tetrachloride, according to the mechanism proposed below.[88] Precisely, appearance of a CTTS band located in the near-UV visible region was demonstrated with ferrocene, resulting from the oxidation of ferrocene to ferrocenium.[89–91]

$$Fc + CCl_4 \rightleftharpoons \underbrace{[Fc,CCl_4]}_{\text{D/A complex}} \xrightarrow{h\nu} Fc^{\oplus} + CCl_4^{\bullet -}$$

By exciting in this absorption band, a photoinduced electron transfer from ferrocene towards the electron accepting solvent could be demonstrated, enabling the initiation of anionic polymerization. In the present case, due to the electron-withdrawing ability of the different electron acceptors, a red-shift of the CTTS band can be expected and absorption maxima varying between 400 and 500 nm could be determined for dyads **D–A*x***, x = 0–11 and triads **A–D–A*x***, x = 0–11, after evolution of their UV-visible absorption spectra. Besides, monitoring of the cyclic voltammograms of **A–D–A0** over time in DMSO and by using tetrabutylammonium hexafluorophosphate as the supporting electrolyte revealed that the new product(s) can be more easily oxidized than the initial dye; the oxidation process being detected at lower anodic potentials (see Fig. 8). Therefore, formation of a ferrocenium cation in DMSO cannot be excluded. However, the oxidation of ferrocenium cation should be more difficult than that of ferrocene due to the loss of one electron. To support the electrochemical process detected in solution, the formation of ferrocenium decomposition products can be tentatively proposed. It is noteworthy that the distinction between ICT and CTTS can be easily done for the following reasons. First, even if a solvatochromism is observed, ICT bands are observed at almost the same positions, irrespective of the solvents. This point has been demonstrated in the solvatochromic study. Conversely, since CTTS is a less kinetically favorable process, it can be monitored over time and is not observed immediately after dissolution of the compound. Therefore, positions of the ICT bands given in the solvatochromic study are the correct ones, corroborated by the similarity of values observed in the twenty-three solvents.

Interestingly, while a clear modification of the UV-visible absorption spectra of the push–pull dyes was determined in DMSO, conversely, for ferrocene, no modification of the absorption spectrum was found in DMSO and even in the twenty-two solvents, evidencing a specific activation process originating from the presence of the electron-withdrawing groups in dyads and triads. In light of these results and considering that an interaction between the solvent and the push–pull dyes exists, several hypotheses were examined, notably with **A–D–A0** as the

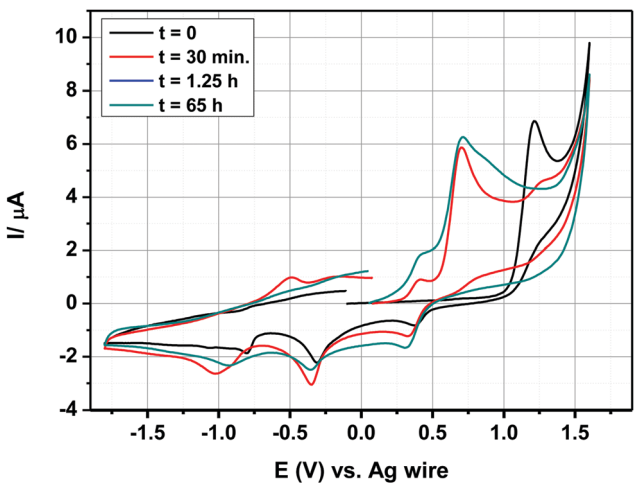

Fig. 8 Cyclic voltammograms of **A–D–A0** over time in DMSO solution at room temperature.

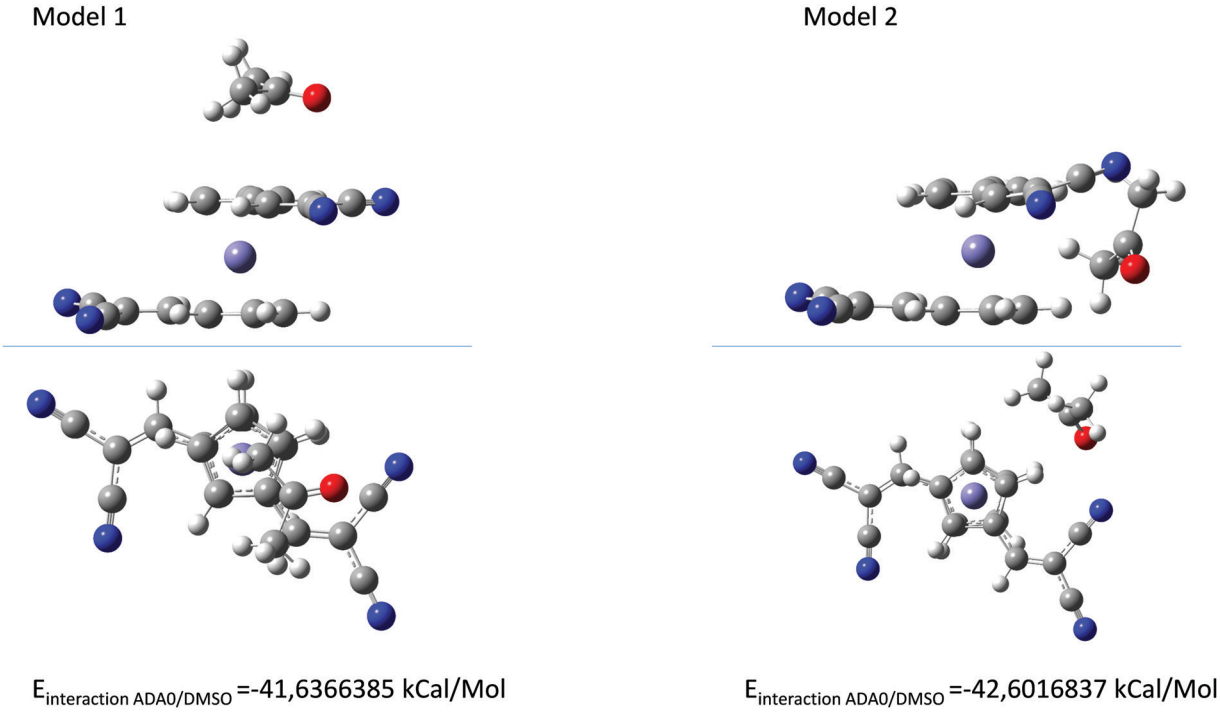

Fig. 9 The two possible interactions between **A–D–A0** and DMSO with DMSO on top of the ferrocene unit (model 1) and DMSO in the lateral position (model 2).

model compound. Thus, interactions between ferrocene in the neutral form and DMSO was examined by positioning the DMSO molecule on top or in lateral position with regards to the ferrocene unit. Calculations done with density-functional theory (DFT) using ωb97xd/6-311++g(d,p) as the basis set revealed that similar energies could be determined in the two situations (see Fig. 9).

As shown in Fig. 9, the energy difference between solvent molecules standing on top or in lateral position to the ferrocene group is negligible. Consequently, considering that the energy difference is low, no preferential orientations can be expected. Interestingly, a blue-shift of the theoretical UV-visible absorption spectra compared to that determine for **A–D–A0** under vacuum conditions could be determined in these two situations.

Possibility of bimolecular interactions between **A–D–A0** molecules was also envisioned. Besides, in this case, a red-shift of the absorption spectra should be observed for the dimers, which is in contradiction with what is experimentally observed (see Fig. 10). Indeed, by theoretical calculations, a maximum absorption around 600 nm is expected, which is not experimentally observed. Besides, from an energy viewpoint, such interactions can theoretically exist. Therefore, based on the different investigations, the formation of a CTTS or the formation of dimers in solutions cannot be proposed as plausible explanations supporting the experimental results. Evolution of the UV-visible absorption spectra over time is also not the result of photoinduced reactions, as similar modifications of the UV-visible absorption spectra over time are detected in the dark and under ambient light.

3.3. Solvatochromism

Solvatochromic behaviors of dyads **D–A*x***, x = 0–11 and triads **A–D–A*x***, x = 0–11 were measured at room temperature in 22 common organic solvents ranging from nonpolar to highly polar solvents. A summary of the optical properties is provided in Tables 4 and 5. Intramolecular nature of the charge transfer detected for the dyads **D–A*x***, x = 0–11 was demonstrated by performing successive dilutions of the solutions and linear correlations between the intensity of the ICT bands and the concentrations could be established. Over the years, numerous empirical polarity scales have been developed to interpret the solvent–solute interaction and the Kamlet–Taft's,[92] Dimroth-Reichardt's,[93] Lippert–Mataga's,[94] Catalan's,[95] Kawski-Chamma Viallet's,[96] McRae Suppan's[97] and Bakhshiev's[98] scales are the most widely used. Among the different empirical polarity scales examined, the solvent polarity/polarizability Catalan (SPP) scale and the Kamlet–Taft polarity scale were determined to be highly useful for analyzing the solvatochromic behaviors of dyads **D–A*x***, x = 0–11.

More precisely, in the case of the Kamlet–Taft empirical scale, better linear correlations were obtained while using a multiparameter approach instead of plotting ΔE = f (π^*) (see Table S2 and S3 in the ESI†). However, it is noteworthy that the multiparameter approach better interprets the solvatochromic behaviors of **D–A*x***, x = 0–7 than of **D–A*x***, x = 8–11. Indeed, for these four dyes, the linear correlations $\Delta E = f(\pi^*)$ were more adapted with regards to their larger values for the square of the correlation coefficient (R^2). In fact, when using the multiparameter approach, two parameters are considered in addition to the dipolarity/polarizability π^*, namely, the

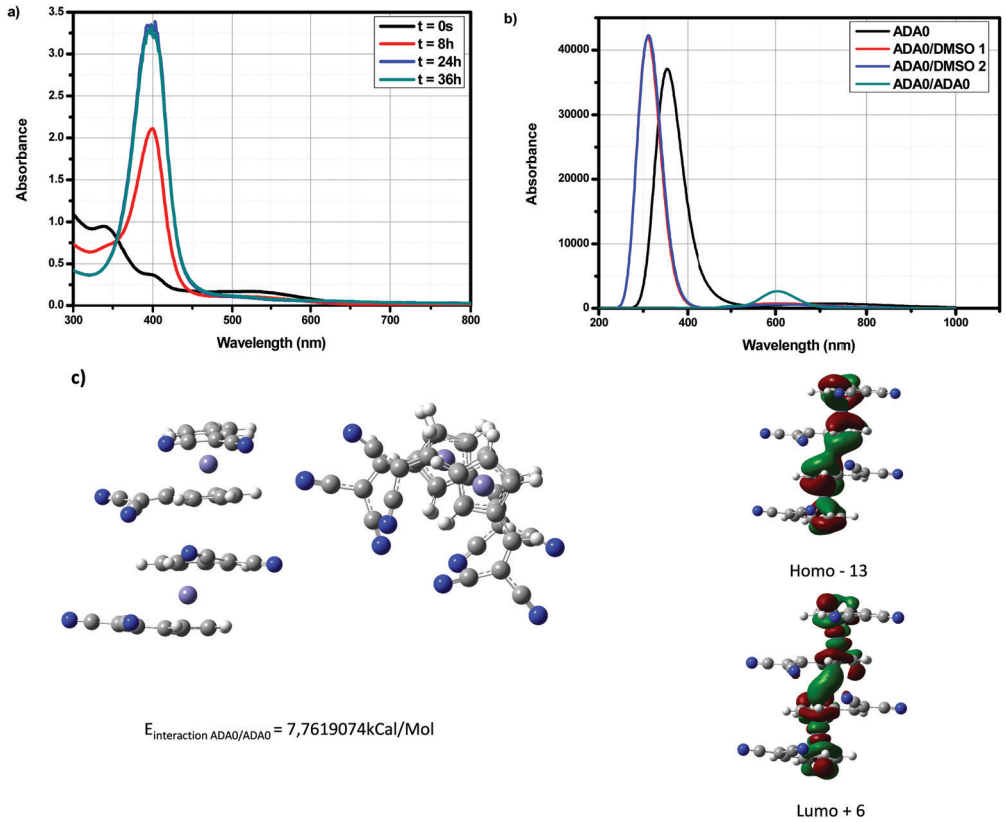

Fig. 10 (a) UV-visible absorption spectra of **A–D–A0** over time in DMSO. (b) Theoretical UV-visible absorption spectra of **A–D–A0** in DMSO and (c) geometrical optimization for **A–D–A0** dimers and contour plots for HOMO−13 and LUMO+6.

hydrogen bond-donating ability α and the hydrogen bond-accepting ability β. These two parameters are of crucial importance in the case of dyes with electron acceptors comprising NH groups such as **D–A6** and **D–A7**. The same holds true for dyes bearing cyano groups such as **D–A0**, **D–A2**, **D–A3**, and **D–A4**, carbonyl groups such as **D–A1**, **D–A8** and **D–A11** or polar groups such as nitro groups. In these different cases, hydrogen bonds can be formed with the precited groups. Conversely, for **D–A9**

Table 4 Summary of the optical properties of **D–Ax**, x = 0–11 in twenty-two solvents and Kamlet and Taft parameters π*

Compounds	π* [a]	D–A0 [b]	D–A1 [b]	D–A2 [b]	D–A3 [b]	D–A4 [b]	D–A5 [b]	D–A6 [b]	D–A7 [b]	D–A8 [b]	D–A9 [b]	D–A10 [b]	D–A11 [b]
Acetone	0.71	524	565	624	612	611	606	565	545	534	571	544	535
Acetonitrile	0.75	528	566	617	614	618	598	573	537	536	572	545	538
AcOEt	0.54	523	563	615	607	602	609	566	543	529	567	544	531
Anisole	0.73	530	567	617	616	619	619	575	552	536	575	548	539
Chloroform	0.78	533	573	631	619	629	607	585	564	543	581	558	543
Cyclohexane	0.00	516	554	613	617	591	643	n.s.[c]	n.s.[c]	514	560	538	514
1,2-Dichloroethane	0.81	531	569	627	611	627	624	582	558	537	574	550	540
Dichloromethane	0.82	530	569	628	620	628	609	584	561	541	578	551	542
Diethyl carbonate	0.45	523	560	626	608	594	602	565	542	529	567	542	529
Diethyl ether	0.27	523	559	617	617	603	613	560	542	524	567	540	526
1,4-Dioxane	0.55	519	562	616	607	596	596	564	544	532	567	543	530
Dimethylacetamide	0.88	530	572	626	627	619	595	567	544	526	579	547	530
DMF	0.87	529	571	624	616	622	584	566	545	526	576	546	529
DMSO	1.00	531	575	626	620	628	591	572	548	524	579	550	526
Ethanol	0.54	528	569	624	616	625	591	570	553	538	576	n.s.[c]	536
Heptane	−0.08	515	554	612	613	585	n.s.[c]	n.s.[c]	n.s.[c]	511	557	538	513
Nitrobenzene	1.01	534	573	639	625	636	605	581	558	543	580	557	545
Pentane	−0.09	512	551	611	609	n.s.[c]	605	n.s.[c]	n.s.[c]	512	556	534	515
THF	0.58	525	565	620	622	607	609	567	543	531	572	545	533
Toluene	0.54	525	565	620	616	602	616	572	551	530	572	545	529
Triethylamine	0.14	519	558	n.s.[c]	n.s.[c]	597	n.s.[c]	567	n.s.[c]	519	n.s.[c]	564	522
p-Xylene	0.43	522	562	617	618	593	614	570	550	527	574	543	529

[a] Kamlet and Taft parameters. [b] Position of the ICT bands are given in nm. [c] n.s.: not soluble.

Table 5 Summary of the optical properties of **A–D–Ax**, x = 0–11 in twenty-two solvents and Kamlet and Taft parameters π*

Compounds	π* [a]	A–D–A 0 [b]	A–D–A 1 [b]	A–D–A2 [b]	A–D–A 3 [b]	A–D–A 4 [b]	A–D–A 5 [b]	A–D–A 6 [b]	A–D–A 7 [b]	A–D–A 8 [b]	A–D–A 9 [b]	A–D–A 10 [b]	A–D–A 11 [b]
Acetone	0.71	437, 525	562	539	631	597	617	608	545	467, 537	487, 572	451, 546	478, 526
Acetonitrile	0.75	392, 522	566	429, 532	628	603	614	596	537	473, 538	482, 576	457, 547	492, 516
AcOEt	0.54	438, 525	562	br. band	626	402, 426, 583	602	n.s.[c]	543	541	479, 571	454, 558	468, 539
Anisole	0.73	442, 534	568	557, 603	637	n.s.[c]	609	584, 613	552	537	480, 585	458, 556	473, 536
Chloroform	0.78	445, 530	573	580	632	600	n.s.[c]	n.s.[c]	564	474, 536	480, 568	459, 557	475, 529
Cyclohexane	0.00	429, 521	555	n.s.[c]	624	n.s.[c]	n.s.[c]	n.s.[c]	n.s.[c]	n.s.[c]	471, 583	n.s.[c]	522
1,2-Dichloroethane	0.81	443, 531	569	557, 624	637	593, 614	620	n.s.[c]	558	470, 536	484, 565	462, 550	475, 536
Dichloromethane	0.82	445, 527	n.s.[c]	574	637	606	620	n.s.[c]	561	470, 536	484, 580	460, 554	478, 538
Diethyl carbonate	0.45	436, 526	562	574	626	580	602	n.s.[c]	542	530	472, 576	453, 559	463, 536
Diethyl ether	0.27	434, 526	559	n.s.[c]	626	n.s.[c]	602	n.s.[c]	542	524	n.s.[c]	n.s.[c]	467, 520
1,4-Dioxane	0.55	437, 523	564	br. band	632	577	596	473, 562	544	537	474, 572	452, 547	475, 536
Dimethylacetamide	0.88	529	573	544, 650	699	401, 468, 617	624	575	543	493, 522	480, 582	467, 561	439, 545
DMF	0.87	528	571	441, 521	608	399, 459, 618	n.s.[c]	570	545	502, 521	br. band	461, 557	504, 520
DMSO	1.00	399, 533	574	440, 535	599	401, 466, 611	n.s.[c]	580	548	502, 521	491, 580	467, 553	501, 521
Ethanol	0.54	439, 522	575	424, 498	588	398, 449, 611	593	563	553	542	478, 578	474, 553	474, 532
Heptane	−0.08	428, 520	553	n.s.[c]	n.s.[c]	n.s.[c]	n.s.[c]	n.s.[c]	n.s.[c]	n.s.[c]	n.s.[c]	n.s.[c]	516
Nitrobenzene	1.01	529	574	br. band	633	592, 633	642	n.s.[c]	558	478, 547	486, 586	591, 638	484, 561
Pentane	−0.09	559	552	n.s.[c]	n.s.[c]	n.s.[c]	n.s.[c]	n.s.[c]	n.s.[c]	n.s.[c]	n.s.[c]	n.s.[c]	507
THF	0.58	435, 524	564	555	633	594	608	470, 581	543	538	474, 595	452, 544	468, 542
Triethylamine	0.14	503	559	n.s.[c]	621	n.s.[c]	n.s.[c]	n.s.[c]	n.s.[c]	n.s.[c]	n.s.[c]	n.s.[c]	527
Toluene	0.54	441, 529	564	587	630	413, 578	594	n.s.[c]	551	528	477, 581	454, 558	467, 538
p-Xylene	0.43	440, 524	563	587	630	418, 598	600	n.s.[c]	550	516	471, 577	453, 562	471, 536

[a] Kamlet and Taft parameters. [b] Position of the ICT bands are given in nm. [c] n.s.: not soluble.

and **D–A10**, alkylation of the NH groups drastically reduces the sensitivity to the hydrogen-bonding ability of the solvents. Among all dyes, the best correlations were obtained for **D–A0**, **D–A1**, **D–A8** and **D–A11**, with $R^2 > 0.88$ (see Fig. 11). While comparing the results obtained with the linear correlations based on the Catalan and the Kamlet–Taft empirical scales, higher R^2 values were obtained with the Catalan SPP parameters, indicating that the polarity/polarizability of the solvents governs the solvatochromism of these dyes. These results were confirmed with the multiparameter approach of the Kamlet–Taft polarity scale for which R^2 similar to that obtained with the Catalan SPP parameter could be determined. Surprisingly, a positive solvatochromism was found for all dyes except for **D–A5** for which a negative solvatochromism was determined (see Fig. 12). This behavior is relatively unusual but is sometimes observed for dyes such as merocyanines.[99,100] The pronounced negative solvatochromism observed for **D–A5** can be assigned to a highly dipolar electronic ground state and a considerably less dipolar first excited state. With increase in the polarity of the medium, the dipolar ground state was more stabilized than the first excited state so that a hypsochromic shift of the ICT band can be observed.[101] The highly polar ground state of **D–A5** can be assigned to the exceptional electron-withdrawing ability of TNF; this acceptor is the strongest electron-acceptor reported to date.[102] It is noteworthy that **D–A5** has previously been examined for its solvatochromic properties according to the literature.[103] However, in this work reported in 2001 by Perepichka and coworkers, the authors already mentioned the complexity of the solvatochromism of this TNF-based dye. Indeed, the Kamlet–Taft or the Reichardt parameter were determined not to be satisfactory to investigate the solvatochromic behavior. Notably, the authors evidenced that the four-parameter Koppel–Palm equation was even unable to rationalize the solvatochromic behavior of **D–A5**.[104–106] In the present case and differing from the previous study of Perepichka and coworkers, an acceptable linear correlation was obtained while using the Catalan SPP parameters since a R^2 of 0.73 was obtained with this solvent polarity scale. Therefore, it can be concluded that this dye is exceptionally sensitive to the polarity/polarizability of the solvents (taken into account with the Catalan SPP parameter), more than the solvent dipolarity which is primarily considered by the Catalan SdP parameter.

Complexity of the solvatochromism in **D–A9** can also arise from the unequal contribution of the nitro groups to the mesomeric forms. Indeed, as shown in Fig. 13, the difference of the conjugation length between the electron-donating ferrocene and the nitro groups can support the presence of several ICT bands for **D–A9**, but also the unexpected solvatochromic behavior.

Finally, sensitivity of the ICT bands of dyads **D–Ax**, x = 0–11 to solvent polarity was confirmed by examining the slopes obtained by plotting the HOMO–LUMO gaps *vs.* the Taft parameters. Indeed, a great slope is indicative of a significant charge redistribution upon excitation. In particular, the zwitterionic form is stabilized in highly polar solvents. As shown in Fig. 14, three dyes were more sensitive than the

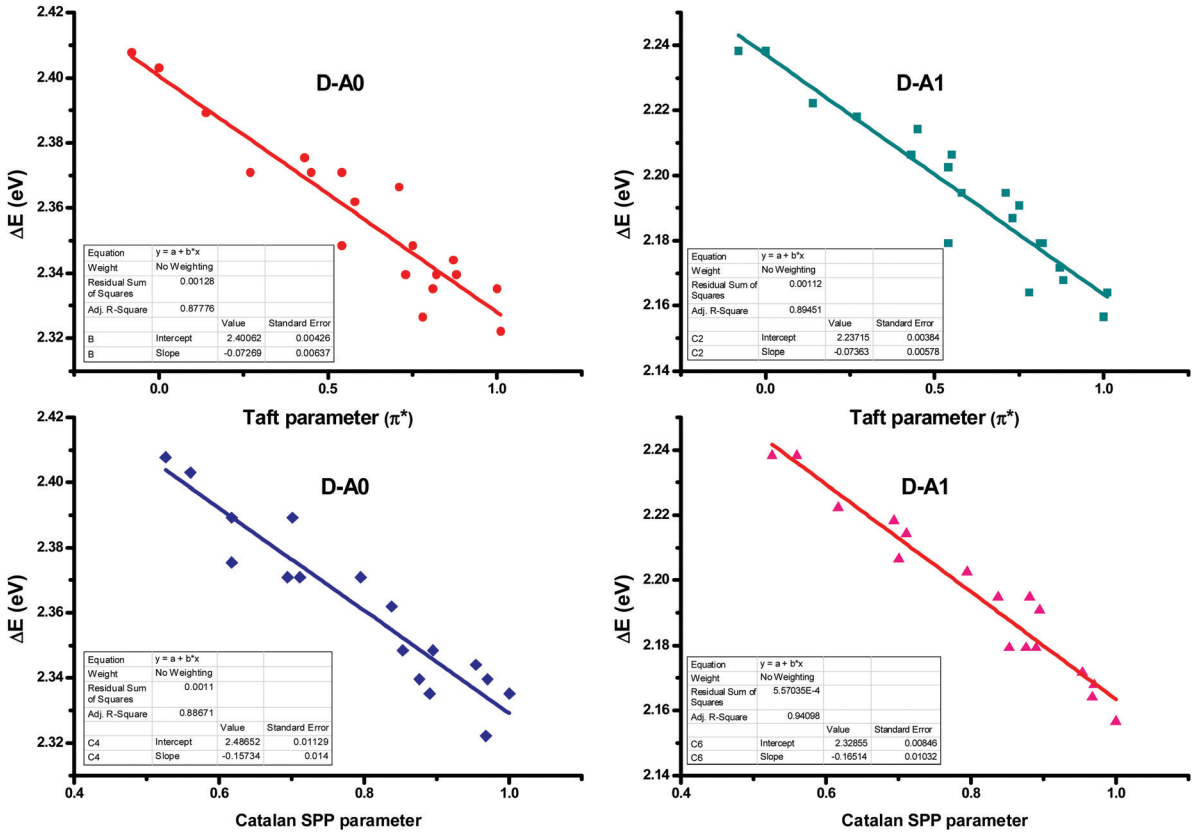

Fig. 11 Linear correlations obtained for **D–A0** and **D–A1** using the Kamlet–Taft and the Catalan empirical scales.

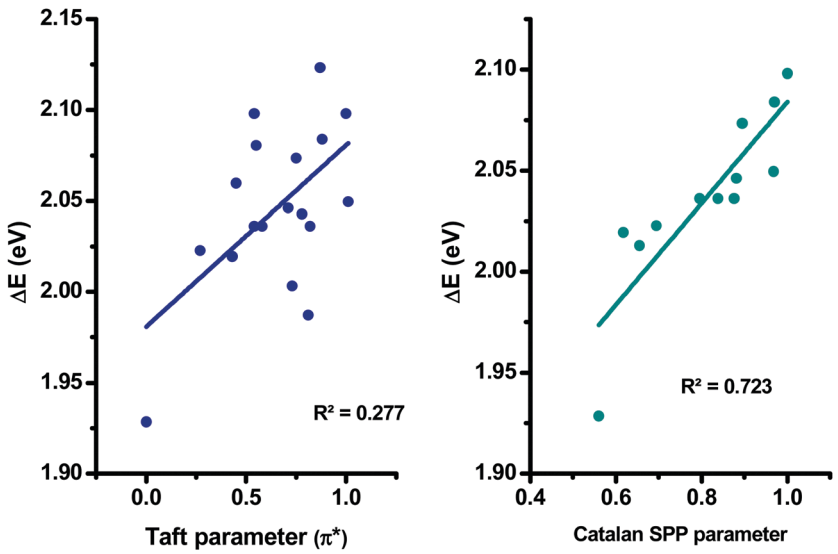

Fig. 12 Linear correlations obtained for **D–A5** using the Kamlet–Taft and the Catalan empirical scales.

others to solvent polarity, namely, **D–A4**, **D–A8** and **D–A11**, comprising TCF or rhodanines as the electron acceptors.

3.4. Electrochemical properties

The two series of compounds examined in this work were analyzed by cyclic voltammetry (CV) in order to determine their electrochemical properties in a dilute solution of dichloromethane. A set of four CV curves is shown in Fig. 15 and all CV curves are given in the ESI.† The redox potentials of all dyes relative to the half-wave oxidation potential of the ferrocene/ferrocenium couple are presented in Table 6.

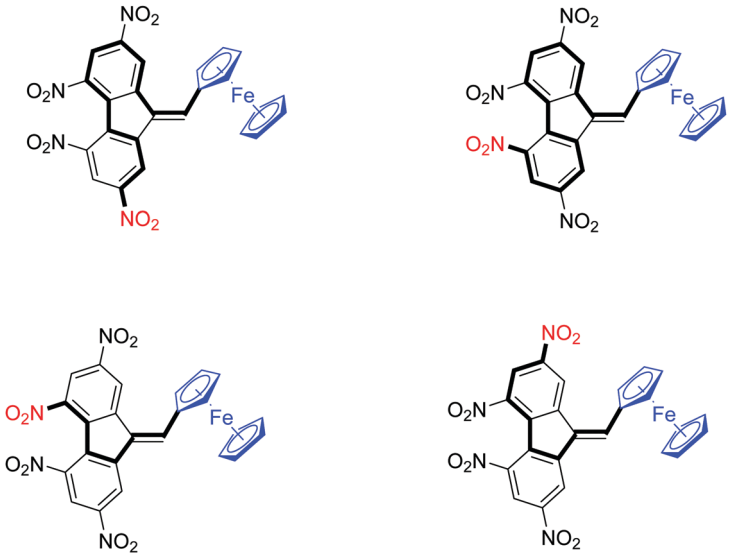

Fig. 13 The different mesomeric forms supporting the presence of two ICT bands for the TNF-based dye **D–A9**.

In this study, the **D–A*x***, x = 0–11 series has exactly the same electron donor as the **A–D–A*x***, x = 0–11 series but differs by the number of electron-accepting groups. As anticipated, major differences could be found concerning their electrochemical properties. Notably, oxidation potentials ranging from + 0.84 V to + 0.60 V could be determined for the **D–A*x***, x = 0–11 series, proving that the oxidation is located on the ferrocene moiety of the push–pull dyes. Indeed, the one-electron oxidation process is detected at low oxidation potentials, comparable to that reported for other push–pull dyes comprising ferrocene as the electron donor.[50,105,106] For **D–A8**–**D–A11**, additional oxidation and reduction peaks were also detected in the region of −0.5 V to 0 V. These additional peaks were specifically observed for the thio(barbituric) and the rhodanine-based dyes. Considering that the different electron acceptors possess amino group, an oxidation process occurring on the amino group with formation of a radical cation can be tentatively proposed. As another explanation, an oxidation of the vinylic spacer followed by a dimerization reaction can also be proposed. Indeed, such oxidation/dimerization reaction has previously been reported in the literature for organic dyes comprising good electron donating groups.[107] For the **A–D–A*x***, x = 0–11 series, a first one-electron process could be determined at higher oxidation potential than that detected for the dyads.

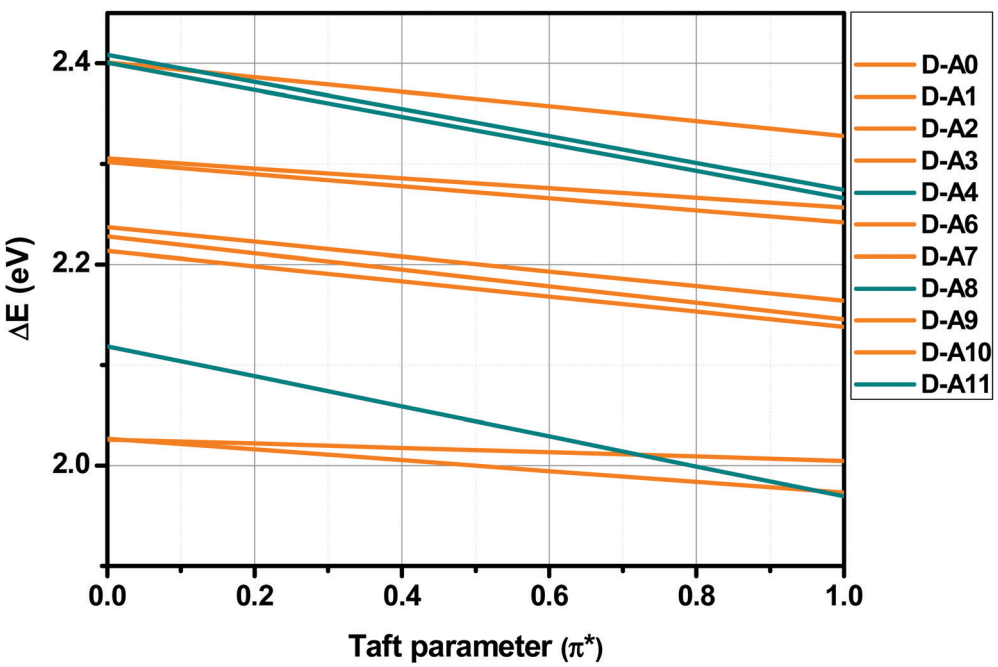

Fig. 14 Variations of the HOMO–LUMO gaps with the Taft parameters.

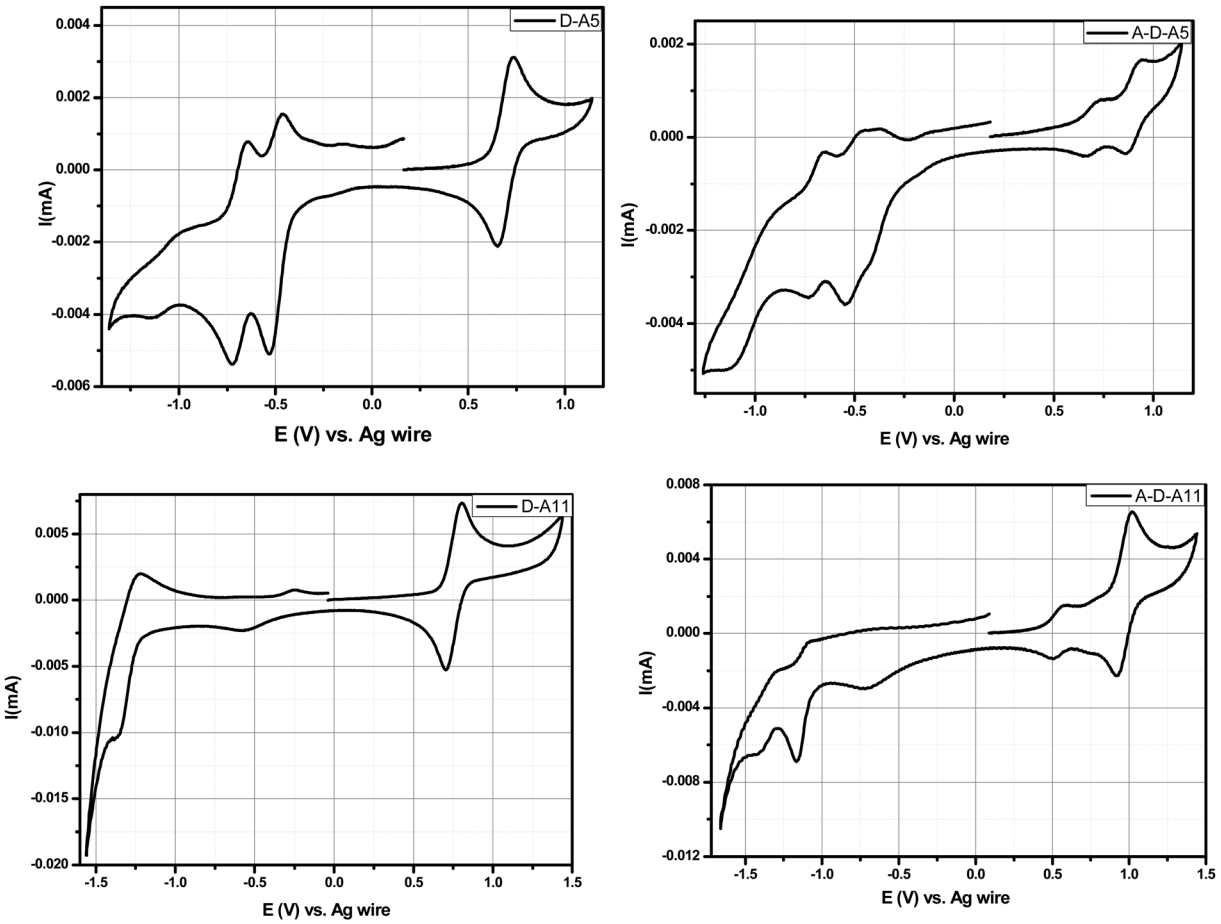

Fig. 15 Comparisons between the cyclic voltammograms of **D–A5/A–D–A5** (up) and **D–A11/A–D–A11** (down) measured in dichloromethane, with tetrabutylammonium perchlorate (0.1 M) as the supporting electrolyte.

Notably, an oxidation located at + 0.51 V for **A–D–A8** to + 1.16 V for **A–D–A0** could be thus determined. In some cases, the presence of a second oxidation process could be detected at anodic potentials, notably, at + 0.90 V for **A–D–A5** and 1.03 V for **A–D–A2**. Similarly, the presence of two or even three reduction potentials could be detected for several dyes, especially for the triads as a result of the presence of two electron-accepting groups.

From their redox potentials, energy levels of the highest occupied molecular orbital (HOMO) and the lowest unoccupied molecular orbital (LUMO) could be estimated using formulas previously reported by Pommerehne *et al.*[108] Values of all HOMO and LUMO energy levels of all molecules are summarized in Table 6. A comparison between the experimental and theoretical values for the HOMO and LUMO energy levels is presented in Fig. 16. In this Figure, a good agreement between the experimental and theoretical results could be evidenced, especially for the **D–A*x***, x = 0–11 series. Conversely, a greater mismatch was found for the **A–D–A*x***, x = 0–11 series, especially for the HOMO energy levels. This can be assigned to the fact that the oxidation process is not only affected by the solvent used to perform electrochemistry but also by the fact that the oxidation process can occur on a specific side of the dye rather than on the ferrocene moiety, as exemplified for the thio(barbituric) or the rhodanine derivatives.

3.5. Redoxchromic properties

Redoxchromism of the two series of compounds was analyzed by UV-visible spectroscopy at a concentration of 8.0×10^{-5} M for all compounds. For all experiments, five equivalents of nitrosonium tetrafluoroborate ($NOBF_4$) were added to the solutions to oxidize ferrocene while maintaining a reasonable acquisition time. Indeed, while using only one equivalent of oxidant, the reaction proved to be relatively slow. Nitrosonium cation is a strong oxidant that is used in numerous chemical reactions and extensively used in Organic Chemistry to oxidize many organic compounds. Indeed, the oxidation potential E° of the nitrosonium cation is lower than 1.7 V (*versus* the normal hydrogen electrode).[109] By oxidizing ferrocene, suppression of the electron donating moiety was clearly evidenced by a color modification of the different solutions. Thus, conversion of the electron-donating ferrocene as an electron acceptor (ferrocenium) induced the disappearance of the intramolecular charge transfer (ICT) band on the UV-visible absorption spectra of the different dyes.

During these analyses, monitoring of the discoloration was performed by recording a spectrum each minute. All spectra are

Table 6 Electrochemical characteristics of the studied compounds **D–Ax**, x = 0–11 and **A–D–Ax**, x = 0–11

	E_{red}	E_{red}	E_{red}	E_{Ox}	E_{Ox}	E_{HOMO}	E_{LUMO}	ΔE_{ET}	ΔE_{opt}
	V/Fc	V/Fc	—	—	V/Fc	eV	eV	eV	eV
D–A0	—	−1.36	—	—	0.84	−5.64	−3.43	2.21	2.33
D–A1	—	−1.27	—	—	0.72	−5.52	−3.52	2.00	2.17
D–A2	—	−0.88	—	—	0.71	−5.51	−3.92	1.60	1.97
D–A3	−0.91	−0.71	—	—	0.60	−5.40	−4.09	1.31	1.98
D–A4	—	−0.86	—	—	0.62	−5.42	−3.94	1.49	1.97
D–A5	−0.68	−0.49	—	—	0.69	−5.49	−4.30	1.19	2.00
D–A6	—	−1.00	—	—	0.80	−5.60	−3.79	1.81	2.13
D–A7	—	−1.17	—	—	0.74	−5.54	−3.63	1.91	2.20
D–A8	—	−1.33	−0.62	−0.30	0.74	−5.55	−3.46	2.08	2.29
D–A9	—	−1.30	−0.63	−0.04	0.71	−5.52	−3.49	2.03	2.13
D–A10	—	−1.39	−0.70	−0.08	0.76	−5.56	−3.40	2.16	2.22
D–A11	—	−1.29	−0.56	−0.23	0.75	−5.55	−3.50	2.05	2.29

	E_{red}	E_{red}	E_{red}	E_{Ox}	E_{Ox}	E_{HOMO}	E_{LUMO}	ΔE_{ET}	ΔE_{opt}
	V/Fc	V/Fc	V/Fc	V/Fc	V/Fc	eV	eV	eV	eV
A–D–A0	—	—	−1.08	1.16	—	−5.96	−3.72	2.25	2.33
A–D–A1	—	−1.13	−0.78	0.85	—	−5.65	−4.02	1.62	2.17
A–D–A2	—	−0.93	−0.63	0.74	1.03	−5.54	−4.17	1.37	2.14
A–D–A3	−1.28	−0.91	−0.60	0.82	—	−5.62	−4.20	1.42	1.97
A–D–A4	—	—	−0.72	0.80	—	−5.60	−4.08	1.52	2.05
A–D–A5	−1.02	−0.69	−0.50	0.70	0.90	−5.50	−4.30	1.20	2.01
A–D–A6	n.s	n.s	n.s	n.s	n.s	n.s	n.s	n.s	n.d
A–D–A7	n.s	n.s	n.s	n.s	n.s	n.s	n.s	n.s	n.d
A–D–A8	—	—	−1.16	0.51	0.97	−5.31	−3.64	1.67	2.31
A–D–A9	n.s	n.s	n.s	n.s	n.s	n.s	n.s	n.s	2.18
A–D–A10	—	—	−1.10	0.83	—	−5.63	−3.70	1.93	2.20
A–D–A11	—	−1.35	−1.11	0.54	0.97	−5.34	−3.68	1.65	2.34

All potentials were recorded in 0.1M $TBAClO_4/CH_2Cl_2$. E_{HOMO} (eV) = $-4.8 - E_{ox}$ and E_{LUMO} (eV) = $-4.8 - E_{red}$.

provided in the ESI.† A panel of three representative kinetics is given in Fig. 17. Interestingly, depending on the electron acceptor, different situations could be clearly identified during the chemical oxidation. As anticipated, a decrease in the intensity of the ICT bands could be detected upon the oxidation of ferrocene as can be observed, as exemplified with compound **D–A2** (see Fig. 17a). For compounds **D–A0**, **D–A1**, **D–A3**, **D–A5**, **A–D–A0**, **A–D–A1**, **A–D–A2**, **A–D–A3**, **A–D–A5** and **A–D–A9**, a similar behavior was observed, with the loss of the ICT band as well as the absorption peaks around 400 nm and 450 nm due to the oxidation of ferrocene to ferrocenium. For the other compounds, a different behavior could be observed, with the appearance during the oxidation process of a new absorption band which eventually decreases after the complete disappearance of the ICT band. This specific behavior can be easily evidenced for **D–A4** (see Fig. 17b), with a decrease in the intensity of the charge transfer band at 640 nm for 10 minutes followed by the appearance of a new absorption band at 560 nm, starting to emerge 7 minutes after the suppression of the ICT band and reaching a maximum of intensity after 14 minutes (see Fig. 17c). Finally, a decrease in the band intensity is then observed and a reduction of half of its initial intensity is observed after one hour of reaction (see Fig. 17d). This behavior is detected for several dyes including **D–A8**, **D–A11**, **A–D–A4**, **A–D–A8** and **A–D–A11.** To a lesser extent, this behavior can also be demonstrated for **D–A6**, **D–A7**, **D–A9**, **D–A10** and **A–D–A10**, except that the appearance of the new absorption band is extremely weak. This behavior is found for the same acceptors irrespective of the series (**D–A** or **A–D–A** series), which is certainly indicative of the presence of side-reactions on the electron acceptor, subsequent to the oxidation of ferrocene to ferrocenium. Thus, for **A–D–A11**, this reaction led to the precipitation of a solid in the solution, resulting in the acquisition of noisy absorption spectra during precipitation (see Fig. 17e).

For this compound, one possible explanation supporting the formation of this precipitate is the polymerization of **A–D–A11** due to the presence of an allyl chain on the electron acceptor. This precipitation is not detected for **D–A11**, also bearing allyl rhodanine as the acceptor. This can be supported by the fact that, in the case of **A–D–A11**, the presence of the two allyl groups allow to form extended chains favoring precipitation. Conversely, in the case of **D–A11**, the presence of a unique polymerizable group per dye only allows the formation of dimers that remain soluble in dichloromethane. From a mechanism viewpoint, several mechanisms can be proposed.

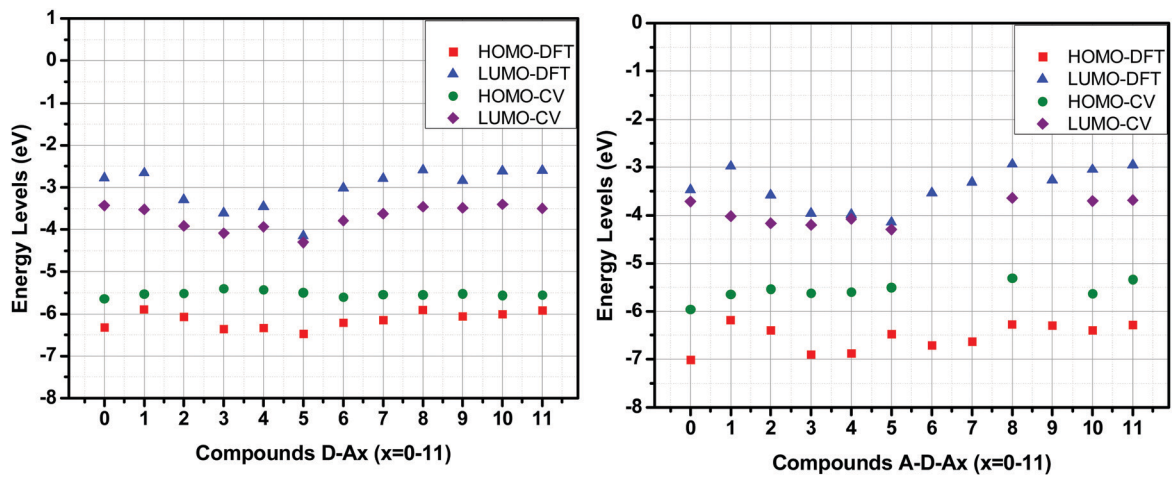

Fig. 16 Comparison of frontier orbitals' energy levels obtained from cyclic voltammetry and DFT calculation.

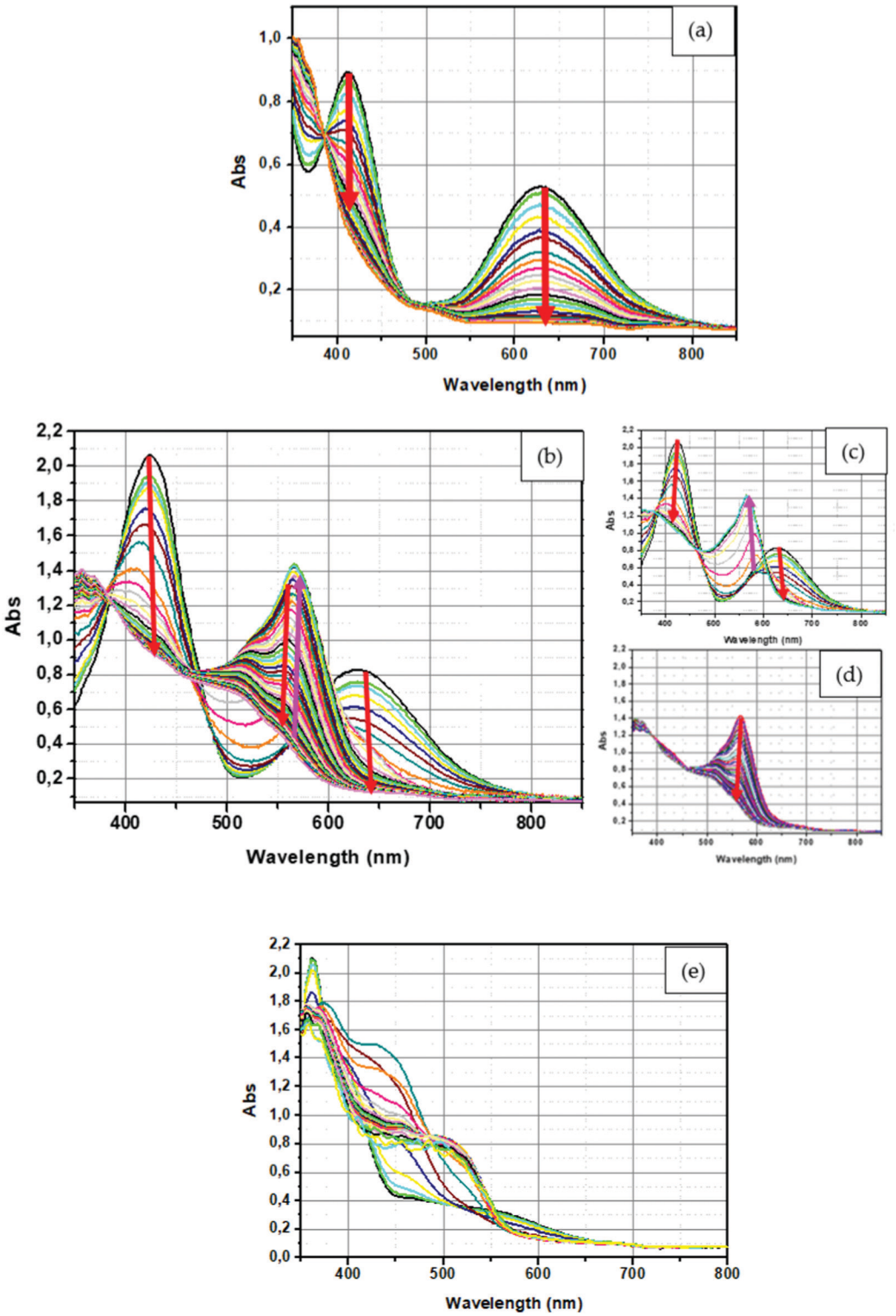

Fig. 17 UV-Visible spectrum of (a) **D–A2**, (b) full spectra of **D–A4** (c) during the first minute for **D–A4**, (d) during the last minute for **D–A4** and (e) **A–D–A11** in dichloromethane.

Notably, polymerization of **A–D–A11** can be induced by an electron transfer reaction between the nitrosonium cation and the allyl function present onto **D–A11** and **A–D–A11** (see Scheme 2a), inducing the formation of radicals and initiating the polymerization or the dimerization process.[110,111] Parallel to this, for **D–A8**, **D–A11**, **A–D–A8** and **A–D–A11**, other reactions are possible on the rhodanine acceptors such as the addition of the nitrosonium cation to the thioether function (see Scheme 2b).

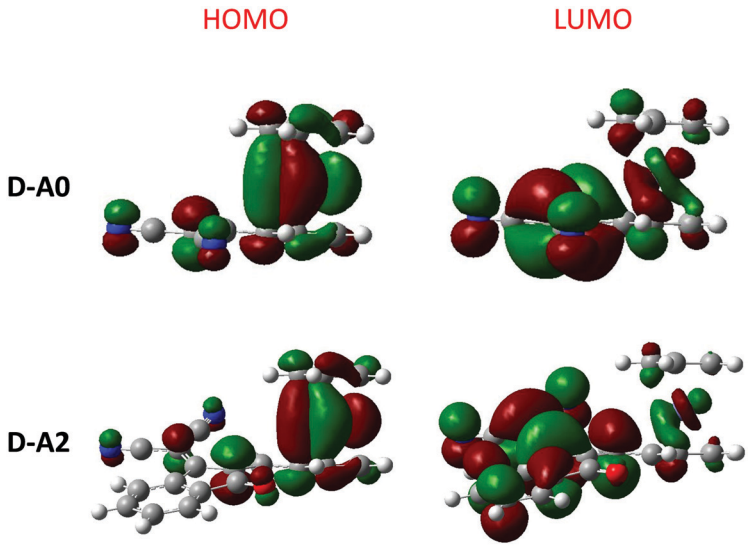

Fig. 18 Contour plots of the electronic distribution of the HOMO and LUMO orbitals of **D–A0** and **D–A2**.

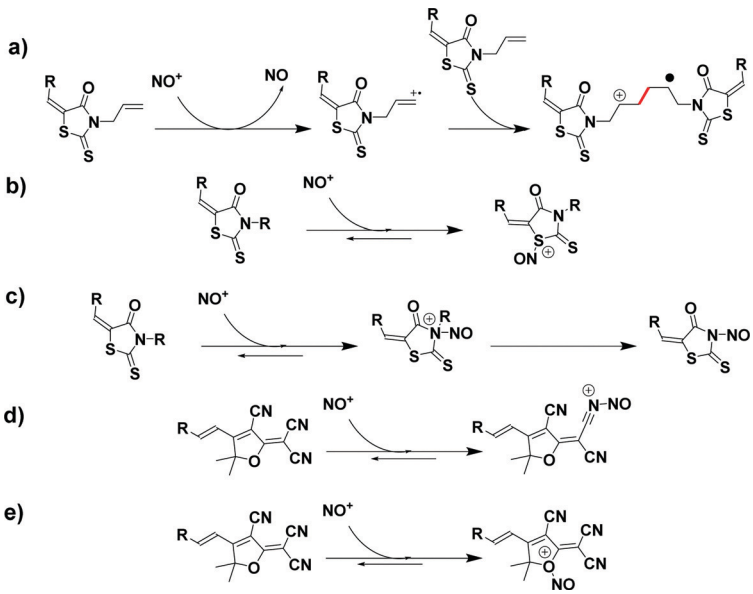

Scheme 2 Proposed reaction occurring with the use of nitrosonium cation on the different functions of the electron acceptor part.

For these rhodanine-based compounds and also for compounds having an amine function, such as **D–A6**, **D–A7**, **D–A9**, **D–A10**, **A–D–A6**, **A–D–A7**, **A–D–A9** and **A–D–A10**, the nitrosation of the amines is also possible, with the addition of the nitrosonium cation leading to a dealkylation of the tertiary amine (see Scheme 2c). Concerning **D–A4** and **A–D–A4**, the two dyes comprise 2-(3-cyano-4,5,5-trimethylfuran-2(5*H*)-ylidene) malononitrile (TCF) as the electron acceptor with numerous cyano groups. In this last case, the nitrosonium cation can also add onto the cyano groups of TCF, modifying its electron-withdrawing ability (see Scheme 2d). Finally, another plausible hypothesis, the nitrosonium cation can also add onto the ether function in a similar way to that observed for the thioether functions of rhodanines (see Scheme 2e). In light of the numerous reactions which can occur between the nitrosonium cation and the electron acceptors, it clearly supports the multiple changes detected in the different absorption spectra during the kinetics of discoloration.

3.6. Theoretical investigations

In light of the unexpected optical properties of the triads, electronic distribution of the highest occupied molecular orbitals (HOMOs) and the lowest unoccupied molecular orbitals (LUMOs) was determined theoretically. DFT calculations were carried out at the B3LYP/6-311G(d,p) level of theory using Gaussian 09 programs. Dichloromethane was used as the

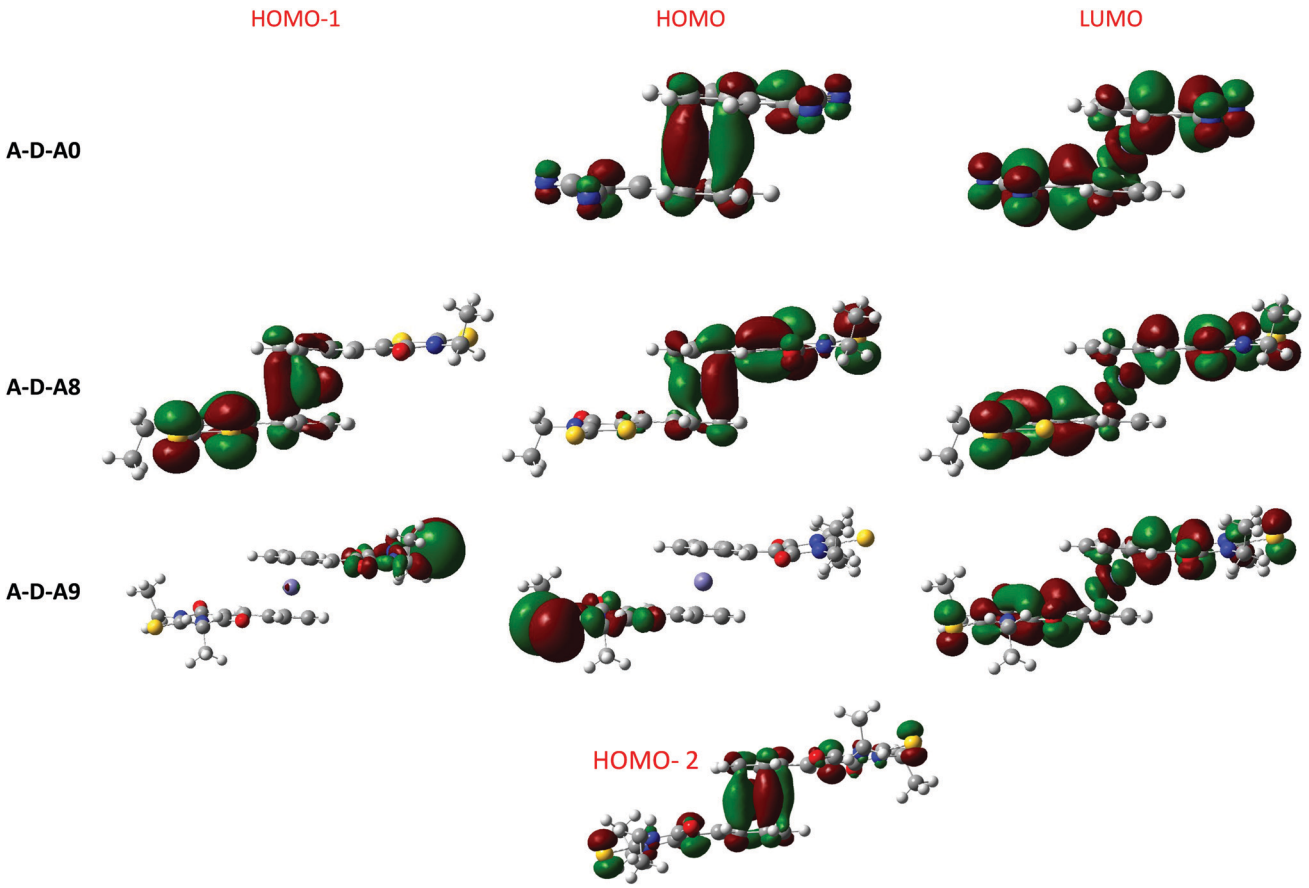

Fig. 19 Contour plots of the electronic distribution of the HOMO and LUMO orbitals of **A–D–A0** and **A–D–A8** and **A–D–A9**.

solvent and the polarizable continuum model (PCM) was used as the solvent model for the TD-DFT calculations.[74–79] More details about the theoretical calculations are given in the ESI.† As shown in Fig. 18, a classical distribution of the molecular orbitals was found for the different dyads, with the HOMO energy level located on the ferrocene moiety and the LUMO energy level on the electron-accepting part. Conversely, an unusual electronic distribution was found for the triads (see Fig. 19). Thus, for **A–D–A*x***, x = 0–7 and **A–D–A10**, a classical electronic distribution could be evidenced. On the contrary, for **A–D–A8** and **A–D–A10**, a HOMO−1 and a HOMO level extending on the ferrocene and the rhodanine moiety was determined. More surprisingly, for **A–D–A9** which possesses the strongest electron-withdrawing group, no electronic distribution of the ferrocene moiety was found neither for the HOMO nor the HOMO−1 energy levels. In fact, HOMO and HOMO−1 levels located onto the TCF moiety were determined. Only an electronic distribution on HOMO−2 can be found on the ferrocene moiety. By theoretical calculations, the energetic transitions involved in the optical transitions could be determined. Thus, as shown in Table 7, all ICT bands are mainly issued from an admixture of a HOMO → LUMO and a HOMO−1 → LUMO transition. These results are consistent with the aforementioned distributions of the electronic density detected for ferrocene. Indeed, HOMO and HOMO−1 are mainly located on the electron donor. These two orbitals are also the highest occupied orbitals, favorable to an electron transfer towards the LUMO level upon excitation.

4. Conclusions

To conclude, a series of twenty-four dyes comprising ferrocene as the electron donor have been designed and synthesized. All dyes showed a strong absorption extending over the visible range. Efficient tuning of the absorption maxima could be achieved not only by means of the number of electron acceptors per dye but also by means of the electron-withdrawing ability. Among the most interesting findings, a positive solvatochromism was found for all dyes, except for the triad comprising the tetranitrofluorene acceptor for which the ground state is more polarized than the excited state. Parallel to this, chemical oxidation of ferrocene in the different dyes suppressed the electron donating ability of ferrocene so that a complete color change of the different solutions could be demonstrated. Use of an excess of nitrosonium cation during the chemical oxidation of ferrocene to ferrocenium induced additional reactions onto the electron acceptors subsequent to the oxidation of ferrocene. Among the most surprising findings, a drastic modification of the UV-visible absorption spectra of the 24 dyes could be

Table 7 Summary of simulated absorption characteristics in dilute dichloromethane of synthesized compounds. Data were obtained in dichloromethane solution

Compounds	E_{HOMO} (eV)	E_{LUMO} (eV)	λ_{max} (nm)	Transitions
D–A0	−6.326	−2.773	669	HOMO−1 → LUMO (64%)
			632	HOMO → LUMO (51%)
			536	HOMO−2 → LUMO (24%)
			500	HOMO → LUMO+1 (62%)
D–A1	−5.887	−2.657	689	HOMO−1 → LUMO (64%)
			653	HOMO → LUMO (54%)
			506	HOMO → LUMO+3 (63%)
D–A2	−6.071	−3.291	744	HOMO−1 → LUMO (57%)
			688	HOMO → LUMO (53%)
			515	HOMO → LUMO (37%)
			513	HOMO → LUMO+3 (45%)
D–A3	−6.360	−3.613	746	HOMO−1 → LUMO+1 (76%)
			683	HOMO → LUMO+1 (67%)
			597	HOMO → LUMO (97%)
			563	HOMO−1 → LUMO (85%)
			507	HOMO → LUMO+3 (48%)
D–A4	−6.336	−3.459	736	HOMO−1 → LUMO (74%)
			687	HOMO → LUMO (62%)
			553	HOMO−3 → LUMO (36%)
			512	HOMO → LUMO+2 (48%)
D–A5	−6.474	−4.150	833	HOMO−1 → LUMO (47%)
			828	HOMO → LUMO (57%)
			642	HOMO → LUMO+4 (29%)
			629	HOMO−1 → LUMO+4 (30%)
			580	HOMO−2 → LUMO (45%)
			547	HOMO−2 → LUMO (40%)
			536	HOMO → LUMO+1 (58%)
			520	HOMO−1 → LUMO+1 (50%)
			502	HOMO → LUMO+2 (85%)
D–A6	−6.207	−3.020	727	HOMO−1 → LUMO (70%)
			669	HOMO → LUMO (60%)
			503	HOMO → LUMO+2 (65%)
			469	HOMO−1 → LUMO+2 (46%)
			424	HOMO−2 → LUMO (95%)
D–A7	−6.145	−2.793	699	HOMO−1 → LUMO (68%)
			652	HOMO → LUMO (56%)
			546	HOMO−2 → LUMO (31%)
			502	HOMO → LUMO+1 (64%)
			456	HOMO+1 → LUMO+1 (45%)
			430	HOMO+1 → LUMO+2 (45%)
D–A8	−5.908	−2.586	646	HOMO−1 → LUMO (49%)
			627	HOMO → LUMO (39%)
			528	HOMO+1 → LUMO+2 (37%)
			506	HOMO → LUMO+2 (52%)
			450	HOMO → LUMO (39%)
			437	HOMO−1 → LUMO (36%)
			413	HOMO−3 → LUMO (94%)
D–A9	−6.063	−2.840	712	HOMO−1 → LUMO (68%)
			663	HOMO → LUMO (57%)
			550	HOMO−4 → LUMO (28%)
			504	HOMO → LUMO+2 (64%)
			468	HOMO−2 → LUMO (89%)
			465	HOMO−1 → LUMO+2 (40%)
			438	HOMO−1 → LUMO+3 (27%)
D–A10	−6.009	−2.613	685	HOMO−1 → LUMO (65%)
			646	HOMO → LUMO (54%)
			542	HOMO−1 → LUMO+1 (27%)
			502	HOMO → LUMO+1 (63%)
			451	HOMO−1 → LUMO+1 (42%)
			427	HOMO−1 → LUMO+2 (27%)
D–A11	−5.920	−2.602	647	HOMO−1 → LUMO (50%)
			628	HOMO → LUMO (39%)
			528	HOMO−1 → LUMO+2 (37%)
			506	HOMO → LUMO+2 (52%)
			451	HOMO → LUMO (39%)
			438	HOMO−1 → LUMO (36%)
			412	HOMO−3 → LUMO (94%)

Table 7 (*continued*)

Compounds	E_{HOMO} (eV)	E_{LUMO} (eV)	λ_{max} (nm)	Transitions
A–D–A0	7.015	−3.465	716	HOMO−1 → LUMO (71%)
			684	HOMO → LUMO (61%)
			563	HOMO−3 → LUMO (39%)
			515	HOMO → LUMO+2 (46%)
			447	HOMO−1 → LUMO+2 (35%)
			419	HOMO → LUMO+1 (51%)
A–D–A1	−6.185	−2.983	745	HOMO−1 → LUMO (69%)
			711	HOMO → LUMO (61%)
			573	HOMO−3 → LUMO (36%)
			529	HOMO → LUMO+5 (38%)
			467	HOMO−1 → LUMO+1 (39%)
			449	HOMO → LUMO+1 (58%)
			428	HOMO−1 → LUMO+1 (47%)
			415	HOMO−1 → LUMO (19%)
A–D–A2	−6.401	−3.577	828	HOMO−1 → LUMO (62%)
			731	HOMO → LUMO (55%)
			596	HOMO−3 → LUMO (30%)
			528	HOMO → LUMO+1 (95%)
			505	HOMO → LUMO+5 (63%)
			503	HOMO−1 → LUMO+1 (93%)
			484	HOMO−1 → LUMO+5 (33%)
			451	HOMO−1 → LUMO+2 (34%)
A–D–A3	−6.901	−3.963	752	HOMO−1 → LUMO (57%)
			715	HOMO → LUMO (49%)
			571	HOMO−4 → LUMO (21%)
			562	HOMO → LUMO+3 (60%)
			523	HOMO → LUMO+2 (62%)
			522	HOMO → LUMO+1 (70%)
			512	HOMO−1 → LUMO+1 (45%)
			508	HOMO−1 → LUMO+2 (56%)
			500	HOMO−1 → LUMO+3 (48%)
			482	HOMO → LUMO+5 (29%)
A–D–A4	−6.877	−3.983	767	HOMO−1 → LUMO (58%)
			733	HOMO → LUMO (59%)
			578	HOMO−4 → LUMO (38%)
			561	HOMO → LUMO+1 (64%)
			502	HOMO−1 → LUMO+1 (55%)
			484	HOMO → LUMO+1 (27%)
			475	HOMO−2 → LUMO (55%)
			458	HOMO−1 → LUMO+4 (32%)
			436	HOMO−4 → LUMO+4 (16%)
A–D–A5	−6.474	−4.150	804	HOMO−1 → LUMO (44%)
			784	HOMO → LUMO (44%)
			677	HOMO → LUMO+1 (89%)
			656	HOMO−1 → LUMO+1 (80%)
			606	HOMO−1 → LUMO (31%)
			600	HOMO → LUMO (24%)
			583	HOMO−4 → LUMO+15 (15%)
			540	HOMO−2 → LUMO (83%)
			538	HOMO−2 → LUMO+1 (58%)
			532	HOMO−2 → LUMO+1 (28%)
			495	HOMO−3 → LUMO (27%)
			484	HOMO → LUMO+3 (70%)
			480	HOMO−3 → LUMO+1 (59%)
			472	HOMO−1 → LUMO+3 (55%)
			471	HOMO → LUMO+2 (42%)
			466	HOMO−1 → LUMO+2 (41%)
			453	HOMO−4 → LUMO (15%)
			447	HOMO → LUMO+5 (47%)
			442	HOMO−1 → LUMO+4 (53%)
			439	HOMO → LUMO+4 (19%)
A–D–A6	−6.709	−3.531	795	HOMO−1 → LUMO (74%)
			734	HOMO → LUMO (64%)
			593	HOMO−6 → LUMO (43%)
			526	HOMO → LUMO+1 (37%)
			476	HOMO−1 → LUMO+1 (46%)
			454	HOMO → LUMO+1 (56%)
			445	HOMO−2 → LUMO (37%)
			444	HOMO−3 → LUMO (37%)

Table 7 (*continued*)

Compounds	E_{HOMO} (eV)	E_{LUMO} (eV)	λ_{max} (nm)	Transitions
			434	HOMO−1 → LUMO+1 (41%)
			415	HOMO−1 → LUMO (17%)
A–D–A7	−6.629	−3.312	766	HOMO−1 → LUMO (74%)
			714	HOMO → LUMO (64%)
			582	HOMO−3 → LUMO (48%)
			519	HOMO → LUMO+2 (46%)
			462	HOMO−1 → LUMO+2 (35%)
			436	HOMO → LUMO+1 (63%)
			418	HOMO−1 → LUMO+1 (56%)
			405	HOMO−1 → LUMO+3 (22%)
A–D–A8	−6.273	−2.934	682	HOMO−1 → LUMO (43%)
			668	HOMO → LUMO (45%)
			548	HOMO−6 → LUMO (27%)
			522	HOMO → LUMO+4 (23%)
			448	HOMO−1 → LUMO+1 (20%)
			444	HOMO → LUMO+1 (59%)
			427	HOMO−1 → LUMO (37%)
			425	HOMO−1 → LUMO+1 (42%)
			420	HOMO−5 → LUMO (41%)
			419	HOMO−4 → LUMO (40%)
A–D–A9	−6.299	−3.264	780	HOMO−3 → LUMO (63%)
			725	HOMO → LUMO (62%)
			586	HOMO−6 → LUMO (44%)
			524	HOMO → LUMO+1 (33%)
			490	HOMO−2 → LUMO (59%)
			489	HOMO−1 → LUMO (58%)
			471	HOMO−3 → LUMO+1 (36%)
			452	HOMO → LUMO+1 (59%)
			432	HOMO−3 → LUMO+1 (40%)
			415	HOMO−3 → LUMO (17%)
A–D–A10	−6.392	−3.049	750	HOMO−1 → LUMO (72%)
			705	HOMO → LUMO (63%)
			576	HOMO−3 → LUMO (44%)
			518	HOMO → LUMO+2 (46%)
			458	HOMO−1 → LUMO+2 (35%)
			433	HOMO → LUMO+1 (63%)
			415	HOMO−1 → LUMO+1 (59%)
			404	HOMO−1 → LUMO+3 (21%)
A–D–A11	−6.289	−2.951	684	HOMO−1 → LUMO (44%)
			670	HOMO → LUMO (46%)
			549	HOMO−6 → LUMO (27%)
			523	HOMO → LUMO+4 (24%)
			450	HOMO−1 → LUMO+1 (21%)
			446	HOMO → LUMO+1 (59%)
			427	HOMO−1 → LUMO (35%)
			426	HOMO−1 → LUMO+1 (41%)
			422	HOMO−3 → LUMO (33%)
			419	HOMO−5 → LUMO (58%)

observed in numerous solvents, and this modification of the UV-visible absorption spectra has never been reported in the literature, even when some of these dyes have been synthesized prior to this work. Although several hypotheses have been examined to support the modification of the absorption spectra over time, isolation and identification of the different reaction products deserve to be investigated in future works. Indeed, although the phenomenon could be clearly evidenced, no clear conclusions could be established concerning the exact origin of these modifications.

Conflicts of interest

There are no conflicts to declare.

Acknowledgements

The authors thank Aix Marseille University and The Centre National de la Recherche Scientifique (CNRS) for financial support. The Agence Nationale de la Recherche (ANR agency) is acknowledged for its financial support through the PhD grant to the VISICAT project of Guillaume Noirbent (ANR-17-CE08-0054). The Direction Générale de l'Armement (DGA)/ Agence Innovation Defense (AID) is acknowledged for its financial support through the PhD grant to Dr Damien Brunel.

References

1 F. Bures, *RSC Adv.*, 2014, **4**, 58826–58851.
2 A. W. Hains, Z. Liang, M. A. Woodhouse and B. A. Gregg, *Chem. Rev.*, 2010, **110**, 6689–6735.
3 Y. Wu and W. Zhu, *Chem. Soc. Rev.*, 2013, **42**, 2039–2058.
4 J. N. Clifford, E. Martinez-Ferrero, A. Viterisi and E. Palomares, *Chem. Soc. Rev.*, 2011, **40**, 1635–1646.
5 C. Duan, K. Zhang, C. Zhong, F. Huang and Y. Cao, *Chem. Soc. Rev.*, 2013, **42**, 9071–9104.
6 M. Liang and J. Chen, *Chem. Soc. Rev.*, 2013, **42**, 3453–3488.
7 C. Duan, F. Huang and Y. Cao, *J. Mater. Chem.*, 2012, **22**, 10416–10434.
8 S. Allard, M. Forster, B. Souharce, H. Thiem and U. Scherf, *Angew. Chem., Int. Ed.*, 2008, **47**, 4070–4098.
9 F. Dumur, C. R. Mayer, K. Hoang-Thi, I. Ledoux-Rak, F. Miomandre, G. Clavier, E. Dumas, R. Méallet-Renault, M. Frigoli, J. Zyss and F. Sécheresse, *Inorg. Chem.*, 2009, **48**, 8120–8133.
10 J.-M. Raimundo, P. Blanchard, N. Gallego-Planas, N. Mercier, I. Ledoux-Rak, R. Hierle and J. Roncali, *J. Org. Chem.*, 2002, **67**, 205–218.
11 B. Jędrzejewska, M. Gordel, J. Szeremeta, P. Krawczyk and M. Samoć, *J. Org. Chem.*, 2015, **80**, 9641–9651.
12 W.-J. Shi, P.-C. Lo, A. Singh, I. Ledoux-Rak and D. K. P. Ng, *Tetrahedron*, 2012, **68**, 8712–8718.
13 N. Mohammed, A. A. Wiles, M. Belsley, S. S. M. Fernandes, M. Cariello, V. M. Rotello, M. M. M. Raposo and G. Cooke, *RSC Adv.*, 2017, **7**, 24462–24469.
14 M.-A. Tehfe, F. Dumur, B. Graff, F. Morlet-Savary, D. Gigmes, J.-P. Fouassier and J. Lalevée, *Macromolecules*, 2013, **46**, 3761–3770.
15 M.-A. Tehfe, F. Dumur, B. Graff, F. Morlet-Savary, D. Gigmes, J.-P. Fouassier and J. Lalevée, *Polym. Chem.*, 2013, **4**, 3866–3875.
16 H. Mokbel, S. Telitel, F. Dumur, L. Vidal, D.-L. Versace, M.-A. Tehfe, B. Graff, J. Toufaily, J.-P. Fouassier, D. Gigmes, T. Hamieh and J. Lalevée, *Polym. Chem.*, 2013, **4**, 5679–5687.
17 P. Xiao, M. Frigoli, F. Dumur, B. Graff, D. Gigmes, J.-P. Fouassier and J. Lalevée, *Macromolecules*, 2014, **47**, 106–112.
18 P. Xiao, F. Dumur, B. Graff, L. Vidal, D. Gigmes, J.-P. Fouassier and J. Lalevée, *Macromolecules*, 2014, **47**, 26–34.

19 P. Xiao, F. Dumur, M.-A. Tehfe, D. Gigmes, J.-P. Fouassier and J. Lalevée, *Macromol. Rapid Commun.*, 2013, **34**, 1452–1458.
20 F. Dumur, D. Gigmes, J.-P. Fouassier and J. Lalevée, *Acc. Chem. Res.*, 2016, **49**, 1980–1989.
21 F. Dumur, *Eur. Polym. J.*, 2021, **147**, 110328.
22 F. Dumur, *Eur. Polym. J.*, 2021, **143**, 110178.
23 F. Dumur, *Eur. Polym. J.*, 2020, **139**, 110026.
24 B. Steyrer, P. Neubauer, R. Liska and J. Stampfl, *Materials*, 2017, **10**, 1445.
25 J. Zhang and P. Xiao, *Polym. Chem.*, 2018, **9**, 1530–1540.
26 C. Pigot, G. Noirbent, T.-T. Bui, S. Péralta, D. Gigmes, M. Nechab and F. Dumur, *Materials*, 2019, **12**, 1342.
27 F. Dumur, C. R. Mayer, E. Dumas, F. Miomandre, M. Frigoli and F. Sécheresse, *Org. Lett.*, 2008, **10**, 321–324.
28 A. Guerlin, F. Dumur, E. Dumas, F. Miomandre, G. Wantz and C. R. Mayer, *Org. Lett.*, 2010, **12**, 2382–2385.
29 S. Forget, H. Rabbani-Haghighi, N. Diffalah, A. Siove and S. Chénais, *Appl. Phys. Lett.*, 2011, **98**, 131102.
30 S. Chénais and S. Forget, *Polym. Int.*, 2011, **61**, 390–406.
31 P. N. Prasad and D. J. Williams, in *Introduction to Nonlinear Optical Effects in Molecules and Polymers*, eds. J. Klafter and J. M. Drake, Wiley, New York, 1991, pp. 132–174.
32 H. S. Nalwa and S. Miyata, *Nonlinear Optics of Organic Molecules and Polymers*, CRC Press, New York, 1997.
33 L. R. Dalton, P. A. Sullivan, D. Bale, B. Olbricht, J. Davies, S. Benight, I. Kosilkin, B. H. Robinson, B. E. Eichinger and A. K. Y. Jen, in *Organic Thin Films for Photonic Applications*, eds. W. N. Herman, S. R. Flom and S. H. Foulger, American Chemical Society, Washington DC, 2010, ch. 2, vol. 1039, pp. 13–33.
34 T. Verbiest, S. Houbrechts, M. Kauranen, K. Clays and A. Persoons, *J. Mater. Chem.*, 1997, **7**, 2175–2189.
35 H. S. Nalwa and S. Miyata, *Nonlinear Optics of Organic Molecules and Polymers*, CRC Press, New York, 1997.
36 D. Brunel, G. Noirbent and F. Dumur, *Dyes Pigm.*, 2019, **170**, 107611.
37 R. R. Gagne, C. A. Koval and G. C. Lisensky, *Inorg. Chem.*, 1980, **19**, 2854–2855.
38 M. Patra and G. Gasser, *Nat. Rev. Chem.*, 2017, **1**, 0066.
39 P. Garra, D. Brunel, G. Noirbent, B. Graff, F. Morlet-Savary, C. Dietlin, V. F. Sidorkin, F. Dumur, D. Duché, D. Gigmes, J.-P. Fouassier and J. Lalevée, *Polym. Chem.*, 2019, **10**, 1431–1441.
40 A. Lai, Z. C. Hern and P. L. Diaconescu, *ChemCatChem*, 2019, **11**, 4210–4218.
41 T. Noël and J. Van der Eycken, *Green Process. Synth.*, 2013, **2**, 297–309.
42 J. A. Findlay, J. E. Barnsley, K. C. Gordon ID and J. D. Crowley, *Molecules*, 2018, **23**, 2037.
43 Z. Deng, H. Yu, L. Wang, J. Liu and K. J. Shea, *J. Mater. Chem. A*, 2019, **7**, 15975–15980.
44 M. E. Welker, *Molecules*, 2018, **23**, 1551.
45 G. Kelly, F. Darviche, N. Robertson, T. Gelbrich, M. B. Hursthouse, D. A. Thomas and I. R. Butler, *Inorg. Chem. Commun.*, 2005, **8**, 874–877.
46 P. D. Jarowski, Y.-L. Wu, C. Boudon, J.-P. Gisselbrecht, M. Gross, W. B. Schweizer and F. Diederich, *Org. Biomol. Chem.*, 2009, **7**, 1312–1322.
47 T. Shoji, S. Ito, T. Okujima and N. Morita, *Chem. – Eur. J.*, 2013, **19**, 5721–5730.
48 T. Mochida and S. Yamazaki, *J. Chem. Soc., Dalton Trans.*, 2002, 3559–3564.
49 A. J. Moore, A. Chesney, M. R. Bryce, A. S. Batsanov, J. F. Kelly, J. A. K. Howard, I. F. Perepichka, D. F. Perepichka, G. Meshulam, G. Berkovic, Z. Kotler, R. Mazor and V. Khodorkovsky, *Eur. J. Org. Chem.*, 2001, 2671–2687.
50 D. F. Perepichka, I. F. Perepichka, A. F. Popov, M. R. Bryce, A. S. Batsanov, A. Chesney, J. A. K. Howard and N. I. Sokolov, *J. Organomet. Chem.*, 2001, **637–639**, 445–462.
51 R. Teimuri-Mofrad, K. Rahimpour and A. Poursadegh, *Mater. Chem. Phys.*, 2017, **200**, 384–394.
52 I. Janowska, J. Zakrzewski, K. Nakatani, J. A. Delaire, M. Palusiak, M. Walak and H. Scholl, *J. Organomet. Chem.*, 2003, **675**, 35–41.
53 A. M. Asiri, *Appl. Organomet. Chem.*, 2001, **15**, 907–915.
54 R. Ziessel, P. Retailleau, K. J. Elliott and A. Harriman, *Chem. – Eur. J.*, 2009, **15**, 10369–10374.
55 S. Kaur, M. Kaur, P. Kaur, K. Clays and K. Singh, *Coord. Chem. Rev.*, 2017, **343**, 185–219.
56 K. Kowalski, Ł. Szczupak, J. Skiba, O. S. Abdel-Rahman, R. F. Winter, R. Czerwieniec and B. Therrien, *Organometallics*, 2014, **33**, 4697–4705.
57 L. M. Ombaka, P. G. Ndungu, B. Omondi and V. O. Nyamori, *J. Coord. Chem.*, 2014, **67**, 1905–1922.
58 A. Ghosh, S. Mishra, S. Giri, S. M. Mobin, A. Bera and S. Chatterjee, *Organometallics*, 2018, **37**, 1999–2002.
59 G. Cooke and O. Schulz, *Synth. Commun.*, 1996, **26**, 2549–2560.
60 J. A. Mata, E. Peris, R. Llusar, S. Uriel, M. P. Cifuentes, M. G. Humphrey, M. Samoc and B. Luther-Davies, *Eur. J. Inorg. Chem.*, 2001, 2113–2122.
61 P. Kaur, M. Kaur, G. Depotter, S. Van Cleuvenbergen, I. Asselberghs, K. Clays and K. Singh, *J. Mater. Chem.*, 2012, **22**, 10597–10608.
62 D. Bao, B. Millare, W. Xia, B. G. Steyer, A. A. Gerasimenko, A. Ferreira, A. Contreras and V. I. Vullev, *J. Phys. Chem. A*, 2009, **113**, 1259–1267.
63 G. Gritzner, *Pure Appl. Chem.*, 1990, **62**, 1839–1858.
64 S. Daniele, M. A. Baldo, P. Ugo and G. A. Mazzocchin, *J. Electroanal. Chem.*, 1990, **295**, 95–111.
65 K. Nikos and G. Tsierkezos, *J. Solution Chem.*, 2007, **36**, 289–302.
66 R. M. Nielson, G. E. McManis, L. K. Safford and M. J. Weaver, *J. Phys. Chem.*, 1989, **93**, 2152–2157.
67 B. S. Aytar, J. P. E. Muller, S. Golan, Y. Kondo, Y. Talmon, N. L. Abbott and D. M. Lynn, *J. Colloid Interface Sci.*, 2012, **387**, 56–64.
68 X. Yin, Y. Li, Y. Li, Y. Zhu, X. Tang, H. Zheng and D. Zhu, *Tetrahedron*, 2009, **65**, 8373–8377.
69 H. Tahara, K. Uranaka, M. Hirano, T. Ikeda, T. Sagara and H. Murakami, *ACS Appl. Mater. Interfaces*, 2019, **11**, 1–6.

70 B. Gélinas, D. Das and D. Rochefort, *ACS Appl. Mater. Interfaces*, 2017, **9**, 28726–28736.
71 I. Asselberghs, K. Clays, A. Persoons, A. M. McDonagh, M. D. Ward and J. A. McCleverty, *Chem. Phys. Lett.*, 2003, **368**, 408–411.
72 A. Federman Neto, J. Miller, V. Faria de Andrade, S. Y. Fujimoto, M. M. de Freitas Afonso, F. Costa Archanjo, V. A. Darin, M. L. Andrade e Silva, A. Donizete Lanchote Borges and G. Del Ponte, *Z. Anorg. Allg. Chem.*, 2002, **628**, 209–216.
73 G. G. A. Balavoine, G. Doisneau and T. Fillebeen-Khan, *J. Organomet. Chem.*, 1991, **412**, 381–382.
74 M. J. Frisch; G. W. Trucks; H. B. Schlegel; G. E. Scuseria; M. A. Robb; J. R. Cheeseman; J. A. Montgomery, Jr.; T. Vreven; K. N. Kudin; J. C. Burant; J. M. Millam; S. S. Iyengar; J. Tomasi; V. Barone; B. Mennucci; M. Cossi; G. Scalmani; N. Rega; G. A. Petersson; H. Nakatsuji; M. Hada; M. Ehara; K. Toyota; R. Fukuda; J. Hasegawa; M. Ishida; T. Nakajima; Y. Honda; O. Kitao; H. Nakai; M. Klene; X. Li; J. E. Knox; H. P. Hratchian; J. B. Cross; V. Bakken; C. Adamo; J. Jaramillo; R. Gomperts; R. E. Stratmann; O. Yazyev; A. J. Austin; R. Cammi; C. Pomelli; J. W. Ochterski; P. Y. Ayala; K. Morokuma; G. A. Voth; P. Salvador; J. J. Dannenberg; V. G. Zakrzewski; S. Dapprich; A. D. Daniels; M. C. Strain; O. Farkas; D. K. Malick; A. D. Rabuck; K. Raghavachari; J. B. Foresman; J. V. Ortiz; Q. Cui; A. G. Baboul; S. Clifford; J. Cioslowski; B. B. Stefanov; G. Liu; A. Liashenko; P. Piskorz; I. Komaromi; R. L. Martin; D. J. Fox; T. Keith; M. A. Al-Laham; C. Y. Peng; A. Nanayakkara; M. Challacombe; P. M. W. Gill; B. Johnson; W. Chen; M. W. Wong; C. Gonzalez and J. A. Pople, Gaussian, Inc. Wallingford CT, 2009.
75 C. Lee, W. Yang and R. G. Parr, *Phys. Rev. B: Condens. Matter Mater. Phys.*, 1988, **37**, 785–789.
76 W. J. Hehre, R. Ditchfield and J. A. Pople, *J. Chem. Phys.*, 1972, **56**, 2257–2261.
77 J. Tomasi, B. Mennucci and E. Cances, *THEOCHEM*, 1999, **464**, 211–226.
78 G. Scalmani and M. J. Frisch, *J. Chem. Phys.*, 2010, **132**, 114110.
79 N. M. O'Boyle, A. L. Tenderholt and K. M. Langner, *J. Comput. Chem.*, 2008, **9**, 839–845.
80 J. C. Calabrese, L.-T. Cheng, J. C. Green, S. R. Marder and W. Tam, *J. Am. Chem. Soc.*, 1991, **113**, 7227–7232.
81 S. Barlow, H. E. Bunting, C. Ringham, J. C. Green, G. U. Bublitz, S. G. Boxer, J. W. Perry and S. R. Marder, *J. Am. Chem. Soc.*, 1999, **121**, 3715–3723.
82 Y. Liao, B. E. Eichinger, K. A. Firestone, M. Haller, J. Luo, W. Kaminsky, J. B. Benedict, P. J. Reid, A. K.-Y. Jen, L. R. Dalton and B. H. Robinson, *J. Am. Chem. Soc.*, 2005, **127**, 2758–2766.
83 X. Wu, W. Wu, X. Cui, J. Zhao and M. Wu, *J. Mater. Chem. C*, 2016, **4**, 2843–2853.
84 P. Aranyosi, Zs Csepregi, I. Rusznak, L. Töke and A. Vig, *Dyes Pigm.*, 1998, **37**, 33–45.
85 M. Henary and M. Mojzych, Stability and Reactivity of Polymethine Dyes in Solution, in *Heterocyclic Polymethine Dyes*, eds. L. Strekowski, Topics in Heterocyclic Chemistry, Springer, Berlin, Heidelberg, 2008, vol 14.
86 S. Oancea and O. Drăghici, *Czech J. Food Sci.*, 2013, **31**, 283–291.
87 S. Sipahli, V. Mdhanlall and J. J. Mellem, *Food Sci. Technol.*, 2017, **37**, 209–215.
88 C. T. Sanderson, B. J. Palmer, A. Morgan, M. Murphy, R. A. Dluhy, T. Mize, I. J. Amster and C. Kutal, *Macromolecules*, 2002, **35**, 9648–9652.
89 H. Kunkely and A. Vogler, *J. Organomet. Chem.*, 1998, **559**, 215–217.
90 U. M. Rabie, *Spectrochim. Acta, Part A*, 2009, **74**, 746–752.
91 B. Mallik, *Molecules*, 2005, **10**, 708–727.
92 M. J. Kamlet, J.-L. M. Abboud, M. H. Abraham and R. W. Taft, *J. Org. Chem.*, 1983, **8**, 2877–2887.
93 C. Reichardt, *Chem. Rev.*, 1994, **94**, 2319–2358.
94 E. Lippert, *Z. Naturforsch.*, 1955, **10a**, 541–545.
95 J. Catalan, *J. Org. Chem.*, 1997, **62**, 8231–8234.
96 A. Kawski, *Acta Phys. Polon.*, 1966, **29**, 507–518.
97 P. Suppan, *J. Chem. Soc. A*, 1968, 3125–3133.
98 N. G. Bakshiev, *Opt. Spektrosk.*, 1964, **16**, 821–832.
99 S. Cha, M. G. Choi, H. R. Jeon and S.-K. Chang, *Sens. Actuators, B*, 2011, **157**, 14–18.
100 C. Reichardt, *Chem. Rev.*, 1994, **94**, 2319–2358.
101 H. Lu and S. C. Rutan, *Anal. Chem.*, 1996, **68**, 1381–1386.
102 G. Noirbent and F. Dumur, *Materials*, 2018, **11**, 2425.
103 I. A. Koppel and V. A. Palm, in *Advances in Linear Free Energy Relationships*, eds. N. B. Chapman and J. Shorter, Plenum Press, London, 1972, p. 203.
104 V. A. Palm, *Fundamentals of Quantitative Theory of Organic Reactions*, Khimiya, Leningrad, 1977, p. 109, in Russian.
105 R. Misra, P. Gautam and R. Maragani, *Tetrahedron Lett.*, 2015, **56**, 1664–1666.
106 I. F. Perepichka, D. F. Perepichka, M. R. Bryce, A. Chesne, A. F. Popov, V. Khodorkovsky, G. Meshulamd and Z. Kotler, *Synth. Met.*, 1999, **102**, 1558–1559.
107 F. Dumur, C. R. Mayer, E. Dumas, F. Miomandre, M. Frigoli and F. Sécheresse, *Org. Lett.*, 2008, **10**, 321–324.
108 J. Pommerehne, H. Vestweber, W. Guss, R. F. Mahrt, H. Bässler, M. Porsch and J. Daub, *Adv. Mater.*, 1995, **7**, 551–554.
109 Z. V. Todres, *Ion-Radical Organic Chemistry: Principles and Applications*, 2nd edn, CRC Press, 2008.
110 Y. Zhou, X. Jia, R. Li, Z. Liu, Z. Liu and L. Wu, *Tetrahedron Lett.*, 2005, **46**, 8937–8939.
111 G. I. Borodkin and V. G. Shubin, *Russ. Chem. Rev.*, 2017, **86**, 18–46.

